



# Global urbanicity is associated with brain and behaviour in young people

Jiayuan Xu<sup>1,2</sup>, Xiaoxuan Liu<sup>1</sup> , Qiaojun Li<sup>1</sup> , Ran Goldblatt<sup>5</sup>, Wen Qin<sup>1</sup>, Feng Liu<sup>1</sup> , Congying Chu<sup>2</sup>, Qiang Luo<sup>6,7</sup>, Alex Ing<sup>2</sup>, Lining Guo<sup>1</sup>, Nana Liu<sup>1</sup>, Huaigui Liu<sup>1</sup>, Conghong Huang<sup>1</sup> , Jingliang Cheng<sup>8</sup>, Meiyun Wang<sup>1</sup> , Zuojun Geng<sup>10</sup>, Wenzhen Zhu<sup>11</sup>, Bing Zhang<sup>12</sup>, Weihua Liao<sup>13</sup>, Shijun Qiu<sup>14</sup>, Hui Zhang<sup>15</sup>, Xaojun Xu<sup>1</sup> , Yongqiang Yu<sup>17</sup>, Bo Gao<sup>18</sup>, Tong Han<sup>19</sup>, Guangbin Cui<sup>20</sup>, Feng Chen<sup>1</sup> , Junfang Xian<sup>22</sup>, Jiance Li<sup>23</sup>, Jing Zhang<sup>24</sup>, Xi-Nian Zuo<sup>1</sup> , Dawei Wang<sup>26</sup>, Wen Shen<sup>27</sup>, Yanwei Miao<sup>28</sup>, Fei Yuan<sup>29</sup>, Su Lui<sup>1</sup> , Xiaochu Zhang<sup>1</sup> , Kai Xu<sup>32</sup>, Longjiang Zhang<sup>1</sup> , Zhaoxiang Ye<sup>34</sup>, Tobias Banaschewski<sup>1</sup> , Gareth J. Barker<sup>1</sup> , Arun L. W. Bokde<sup>1</sup> , Herta Flor<sup>38,39</sup>, Antoine Grigis<sup>40</sup>, Hugh Garavan<sup>41</sup>, Penny Gowland<sup>1</sup> , Andreas Heinz<sup>1</sup> , Rüdiger Brühl<sup>44</sup>, Jean-Luc Martinot<sup>1</sup> , Eric Artiges<sup>1</sup> , Frauke Nees<sup>1</sup> , Dimitri Papadopoulos Orfanos<sup>1</sup> , Herve Lemaitre<sup>47</sup>, Tomáš Paus<sup>1</sup> , Luise Poustka<sup>50</sup>, Lauren Robinson<sup>51</sup>, Sarah Hohmann<sup>35</sup>, Juliane H. Fröhner<sup>1</sup> , Michael N. Smolka<sup>1</sup> , Henrik Walter<sup>1</sup> , Robert Whelan<sup>1</sup> , Jeanne Winterer<sup>54,55</sup>, Kevin Patrick<sup>1</sup> , Vince Calhoun<sup>1</sup> , Mulin Jun Li<sup>58</sup>, Meng Liang<sup>59</sup>, Peng Gong<sup>1</sup> , Edward D. Barker<sup>1</sup> , Nicholas Clinton<sup>1</sup> , Andre Marquand<sup>62</sup>, Le Yu<sup>1</sup> , Chunshui Yu<sup>1,63</sup> , Gunter Schumann<sup>1</sup> , the CHIMGEN\* and IMAGEN Consortia\*

**Urbanicity is a growing environmental challenge for mental health.** Here, we investigate correlations of urbanicity with brain structure and function, neuropsychology and mental illness symptoms in young people from China and Europe (total  $n = 3,867$ ). We developed a remote-sensing satellite measure (UrbanSat) to quantify population density at any point on Earth. UrbanSat estimates of urbanicity were correlated with brain volume, cortical surface area and brain network connectivity in the medial prefrontal cortex and cerebellum. UrbanSat was also associated with perspective-taking and depression symptoms, and this was mediated by neural variables. Urbanicity effects were greatest when urban exposure occurred in childhood for the cerebellum, and from childhood to adolescence for the prefrontal cortex. As UrbanSat can be generalized to different geographies, it may enable assessments of correlations of urbanicity with mental illness and resilience globally.

Mental disorders account for 28% of non-communicable disease burden<sup>1</sup>. Environmental factors account for up to 50% of the attributable risk for mental disorders<sup>2</sup>. The environmental measures investigated in mental health research include not only individual life events<sup>3</sup>, such as trauma, abuse, neglect or psychosocial stress, but also, albeit to a lesser extent, individual physical environments<sup>4</sup>.

Urbanicity, the living conditions particular to urban areas, is among the most important environmental challenges globally<sup>5</sup>. While physical environments are hallmarks of a city, urbanicity also includes the social environment and access to health and social services<sup>5</sup>. The physical, social and service dimensions of urbanicity form a complex relation with each other that has hitherto prevented the development of a unifying concept and measure of urbanicity<sup>5</sup>.

In 1950, less than 30% of the world's population lived in urban areas, but this fraction has increased to 55% presently and is expected to rise to 68% in 2050 (ref. <sup>6</sup>). While Europe is among the most stable urbanized regions, Asia is home to 54% of the world's urban population and subject to massive demographic changes. For example, by 2050, China will have added 255 million urban

dwellers<sup>7</sup>. This increasing global urban population emphasizes the importance of investigating how the living conditions particular to urban areas affect human brain and behaviour.

We were interested in investigating the relation of urbanicity with brain and behaviour in different sociocultural conditions and geographies. We also aimed to identify possible susceptibility periods across the life span in young people, enabling targeted preventions when the developing brain may benefit most from environmental modification. Whereas there might be distinct influences of increased population density in urban settings in different sociocultural conditions and geographies, there are likely to exist common associations with brain and behaviour shared in different areas of the globe.

Several studies have focused on the relation of individual physical environments linked to urban living with brain and behaviour, such as green space, air and noise pollution<sup>4,8</sup>. However, a more general measure of urbanicity that can objectively assess urban environment with high spatiotemporal resolution and coverage is still lacking. Such a general measure is important, as it registers the overall and susceptibility period relations of urbanicity with brain and

\*A full list of affiliations appears at the end of the paper.

behaviour, and may in a subsequent step enable the identification and ranking of the individual features of the physical, social and service environment, and their interactions, that contribute most to the observed relation.

Traditionally, characterization of urbanicity was carried out using census data, which are ascertained infrequently in different ways and at different times in different countries<sup>5</sup>. Thus, census data are less useful for comparing urbanicity across different countries. More recently, the Global Human Settlement Layer (GHSL) has provided globally standardized human settlements, including urbanization and urbanicity<sup>9</sup>. GHSL data, however, are only available at large and infrequent intervals, namely 1975, 1990, 2000 and 2015 (ref. <sup>9</sup>).

To facilitate global comparative analyses of the overall relations of urbanicity with brain and behaviour and to identify potential susceptibility periods, dense quantitative and longitudinal environmental measures that can be obtained from different geographies are required. Remotely sensed satellite data provide globally standardized quantitative environmental measures enabling the tracing of environmental features going back nearly 50 years (ref. <sup>10</sup>). Population density is a well-established and quantifiable general measure of urbanicity that is frequently applied for neighbourhood classification and used around the globe<sup>9</sup>. Here, we aimed to use population density as a general measure of urbanicity to investigate whether the urban environment is correlated with brain and behaviour, and if these correlations are comparable in China and Europe. Specifically, we developed a satellite-based measure of population density termed ‘UrbanSat’, and applied it in China and Europe to investigate the relation of population density, as a proxy of urbanicity, with brain structure, function and behaviour in two neuroimaging datasets of young people: as an exploration dataset, we used the Chinese CHIMGEN cohort ([www.chimgen.tmu.edu.cn](http://www.chimgen.tmu.edu.cn))<sup>11</sup>, and as the replication dataset, we used the European longitudinal IMAGEN cohort ([www.imagen-europe.com](http://www.imagen-europe.com))<sup>12</sup>. While we did not have any a priori hypothesis, we were interested in investigating whether: (i) UrbanSat is associated with brain structure, function and behaviour; (ii) brain features associated with UrbanSat mediate the association between UrbanSat and behaviour; (iii) correlations of UrbanSat with brain and behaviour are similar in Chinese and Europeans; Furthermore, we were interested in (iv) identifying susceptibility periods for the relations of UrbanSat during child and adolescent development with brain and behaviour. A schematic summary is shown in Fig. 1.

## Results

**Demographics.** We recruited young-adult participants with lifetime residential geographies from CHIMGEN ( $n=3,306$ ) and IMAGEN second follow-up (FU2) ( $n=561$ ). Detailed inclusion and exclusion criteria are presented in Supplementary Tables 1 and 2. Demographics of the samples used in statistical analyses and sample attrition are described in Supplementary Table 3 and Extended Data Fig. 1. Demographic comparisons between the analysed sample and total sample are shown in Supplementary Table 4. Demographic variables showing significant differences between the analysed sample and excluded sample were adjusted during analyses (Methods and Supplementary Tables 5 and 6).

**UrbanSat: a satellite-based measure of urbanicity.** To develop a satellite-based measure of urbanicity, we selected information from nine types of satellite registrations relevant for detecting and characterizing urban settlements, including night-time light (NL), normalized difference built-up index (NDBI), normalized difference water index (NDWI), normalized difference vegetation index (NDVI) and five measures derived from land cover mapping (built-up%, cropland%, grassland%, forest% and water body%) (Supplementary Table 7). We used multiple imputation by chained equations (MICE) to impute the nine annual satellite registrations

and generate ten complete datasets. The multiple training–test splits of the dataset were performed to ensure that the estimates of generalizability we obtain are unbiased throughout the imputation (Supplementary Table 8, Extended Data Fig. 2 and Methods). We then carried out a tenfold cross-validation to optimize the confirmatory factor analysis (CFA) models, and to predict annual UrbanSat scores of each participant from birth to age of recruitment (Extended Data Fig. 2 and Methods). UrbanSat was generated by the optimized CFA model consisting of NL, built-up%, cropland% and NDVI, which best captured variation of urban features while maximizing goodness of fit. UrbanSat in CHIMGEN and IMAGEN-FU2 had a Tucker–Lewis index and comparative fit index  $> 0.95$ , root-mean-square error of approximation (RMSEA)  $< 0.06$  and standard root-mean-square residual (SRMR)  $< 0.08$ , indicating excellent model fit (Supplementary Table 9 and Methods). UrbanSat was robust across time and geographies, as validated by its correlations with ground-level population density from GHSL-population grid (GHSL-POP)<sup>9</sup> for China and Europe for the years 1990, 2000 and 2015 (Fig. 2). Histograms of the distribution of UrbanSat score in each centre are shown in Extended Data Fig. 3. UrbanSat showed higher correlations with population density in different residential categories (rural, town, city and overall), countries (Asia and Europe) and years (1990, 2000 and 2015) than any individual satellite measures (Fig. 2).

**Correlations of UrbanSat with brain structure.** Voxel-wise multiple regression of mean UrbanSat before age 18 years with brain grey matter volume (GMV) was performed in CHIMGEN ( $n=2,176$ ). We controlled for age in all analyses, thus accounting for the older and wider age spread in CHIMGEN (age  $23.54 \pm 2.33$  years) compared with IMAGEN (age  $18.89 \pm 0.66$  years). We also controlled throughout for gender, education, site, body mass index (BMI), genetic population stratification and socioeconomic status (SES) (Supplementary Tables 10 and 11). Total intracranial volume was controlled in all imaging analyses, except for the analyses of cortical thickness (CT) and surface area (SA), where mean CT and total SA were controlled, respectively. Parental history of mental illness was an exclusion criterion for CHIMGEN and controlled for in IMAGEN. Uncorrected statistical maps of the association of UrbanSat with brain GMV in CHIMGEN adjusting for confounding covariates under parametric testing and non-parametric permutation testing are shown in Fig. 3a and Extended Data Fig. 4. We found negative correlation of UrbanSat with medial prefrontal cortex (mPFC) volume (peak Montreal Neurological Institute (MNI) coordinate:  $x=-1.5$ ,  $y=60$ ,  $z=0$ ; 294 voxels; peak  $t$  value  $-5.63$ ; Fig. 3b) and a positive correlation with cerebellar volume (peak MNI coordinate:  $x=10.5$ ,  $y=-51$ ,  $z=-18$ ; 440 voxels; peak  $t$  value  $6.43$ ; Fig. 3b) (parametric testing  $P_c < 0.05$ , family-wise error (FWE) corrected for voxel numbers, imaging modalities and data categories; see Methods). We confirmed the results with non-parametric permutation testing (threshold-free cluster enhancement (TFCE)-FWE,  $P_c < 0.05$ , Supplementary Methods and Extended Data Fig. 4). Potential imputation bias was ruled out by multiple sensitivity analyses (Methods, Extended Data Fig. 2 and Supplementary Results). Uncorrected and adjusted vertex-wise correlation maps of UrbanSat with whole brain CT and SA are shown in Extended Data Fig. 4 ( $n=2,164$ ). The mPFC region of interest (ROI) from GMV analyses was projected onto fsaverage surface of Freesurfer v5.3.0 (Extended Data Fig. 4). UrbanSat was correlated with mean SA ( $\rho = -0.07$ ,  $P = 0.002$ ) but not mean CT ( $\rho = -0.02$ ,  $P = 0.381$ ) of the mPFC cluster (Fig. 3b and Supplementary Table 12). Using voxel-wise multiple regression of individual satellite measures with GMV, we found significant correlation with mPFC-GMV being driven by NL and built-up%, and correlation with cerebellar-GMV being driven by NL and cropland%. We found no correlation of NDVI with either mPFC- or cerebellar-GMV (Extended Data Fig. 5). We observed similar results

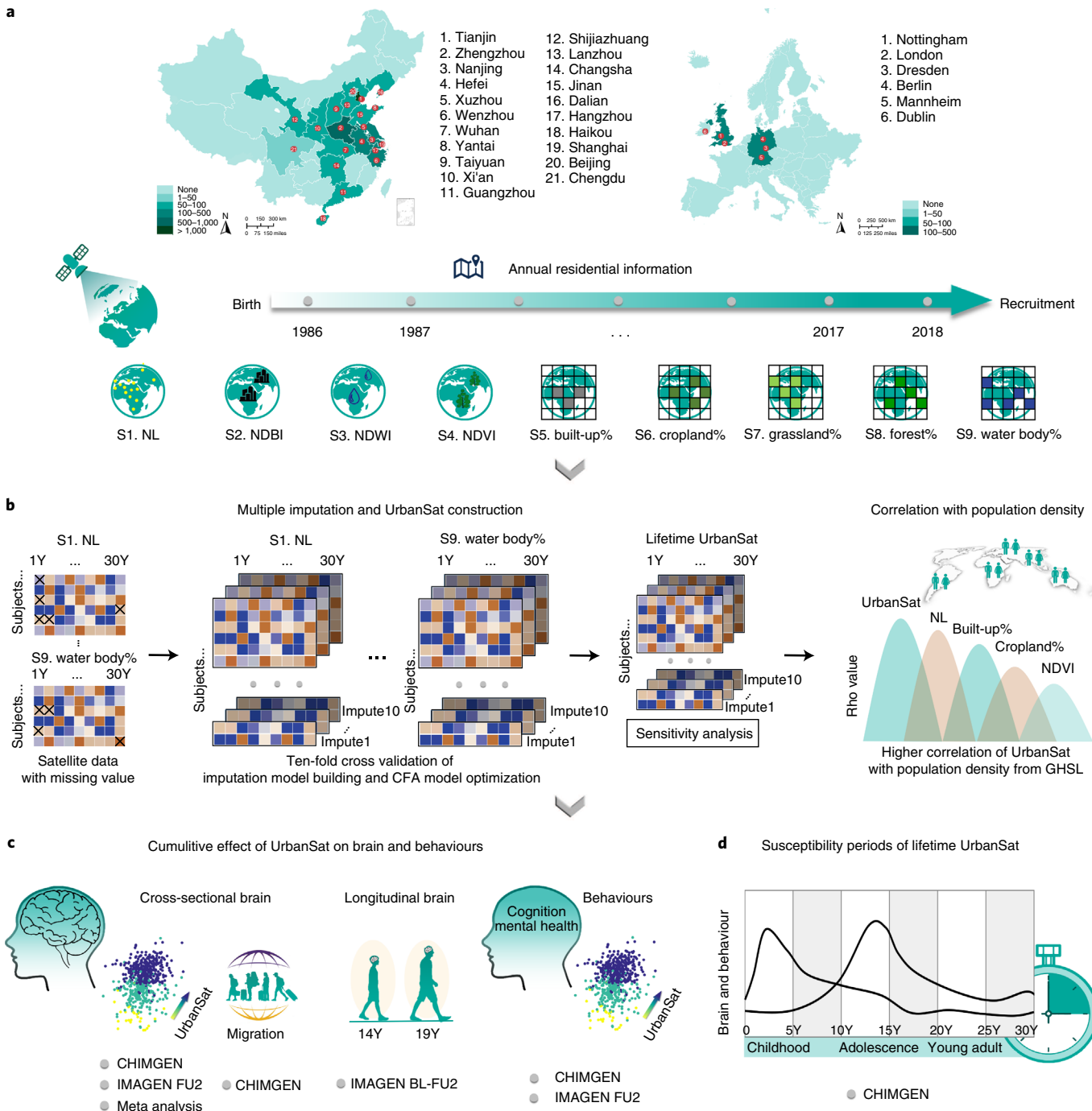


**Fig. 1 | Schematic summary of study design.** **a**, Geographic distribution of recruitment sites and number of participants collected in each city of China and in each country of Europe (top), including five sites in Tianjin, two sites each in Zhengzhou, Nanjing, Hefei and Wenzhou and one site in the remaining cities. Lifetime residential geopositions of each participant collected from 1986 to 2018 (bottom). On the basis of the individual geoposition data, the annual values of nine satellite measures of urbanicity are obtained for each participant, including NL, NDBI, NDWI, NDVI and five measures derived from land cover mapping (built-up%, cropland%, grassland%, forest% and water body%). **b**, Tenfold cross-validation of multiple imputation model building and CFA model optimization for UrbanSat construction. The optimized CFA model includes NL, built-up%, cropland% and NDVI. The mean UrbanSat scores before 18 years showed stronger correlation with ground-level population density from GHSL than any individual satellite measures in both CHIMGEN and IMAGEN-FU2. **c**, Investigation of the cumulative relations of UrbanSat with brain and behaviour. **d**, Identification of susceptibility periods of lifetime UrbanSat on brain and behaviour using distributed lag models. CFA, confirmatory factor analysis; GHSL, global human settlement layers; IMAGEN BL-FU2, IMAGEN BL-FU2 measures brain structural and functional change rate between BL of 14 years and FU2 of 19 years; IMAGEN FU2, IMAGEN second-follow-up-assessment acquired at 19 years of age; NDBI, normalized difference built-up index; NDVI, normalized difference vegetation index; NDWI, normalized difference water index; NL, night-time light; S, satellite measures of urbanicity; Sub, subjects; Y, years old.

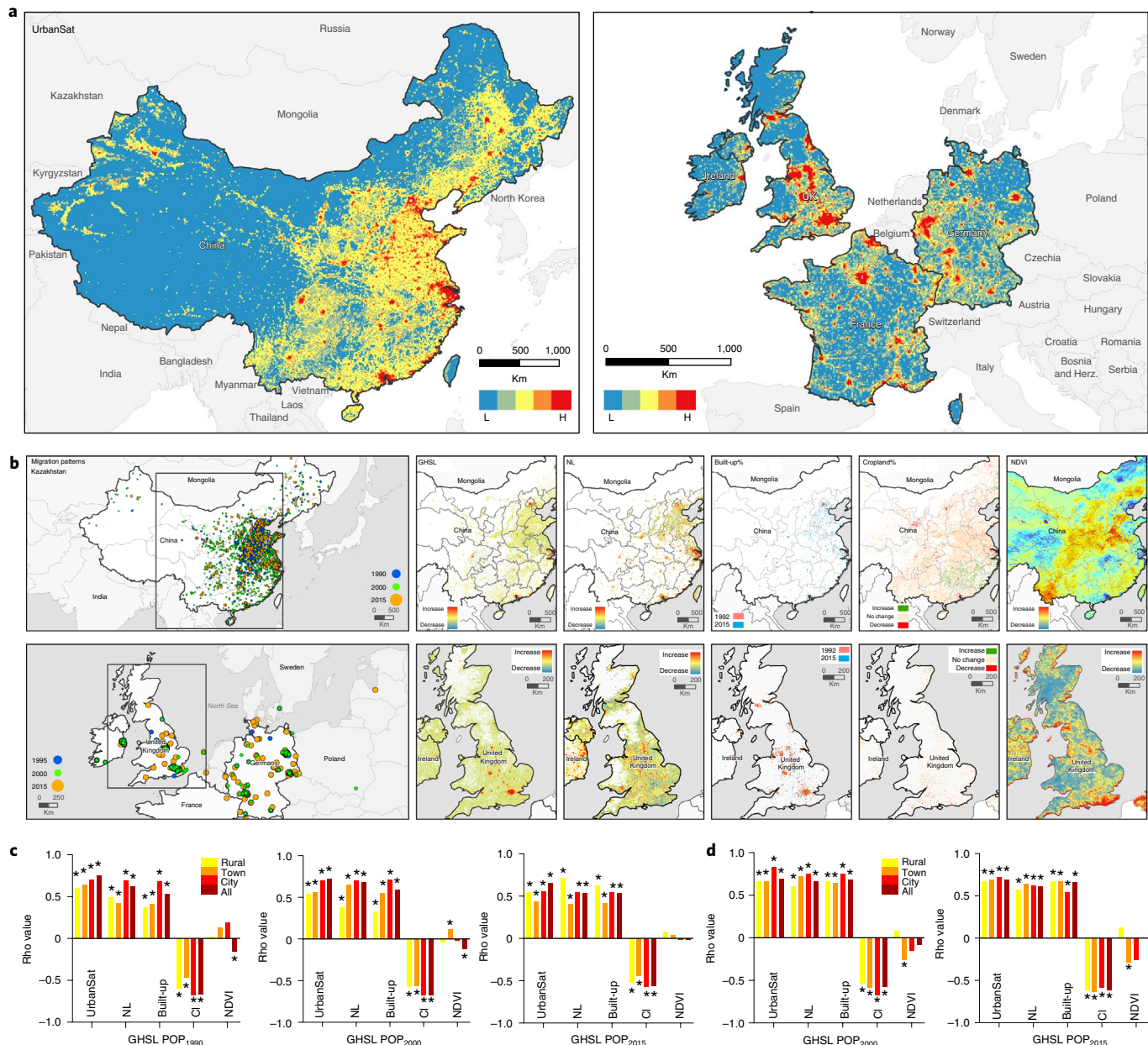


**Fig. 2 | Maps of satellite-based measures of urbanicity in China and Europe.** **a**, UrbanSat maps of China (left) and Europe (right) in 2013. **b**, Maps showing temporal changes of satellite measures of urbanicity during available years in China (top row) and Europe (bottom row). Left, migration patterns of 3,306 participants in CHIMGEN and 561 participants in IMAGEN-FU2. Blue, green and orange dots represent geographic locations of participants in the year 1990, 2000 and 2015, respectively. The box on the map represents the extent of zoom-in maps of each satellite measure of urbanicity in the right columns. Right, Changes of GHSL-population density between 1990 and 2015, NL between 1992 and 2013, built-up% and cropland% between 1992 and 2015 and NDVI between 1981 and 2017 in zoom-in part of China and Europe. Different time ranges are available for different satellite registrations. **c,d**, Correlations of UrbanSat and individual satellite measures with population density in 3,306 CHIMGEN (**c**) and 561 IMAGEN-FU2 (**d**) participants. Columns demonstrate  $\rho$  value (y axis) of the UrbanSat and individual (NL, built-up%, cropland% and NDVI) satellite measures (x axis) with GHSL-population density in rural (yellow), town (orange), city (red) and combined (dark red) in CHIMGEN for the years 1990, 2000 and 2015, and in IMAGEN for the years 2000 and 2015. CI, cropland%. \*Significant correlations of satellite measures of urbanicity with population density using Spearman correlation analysis.

in GHSL ground-level population density data, thus validating the relation of UrbanSat and GMV (Extended Data Fig. 5).

In IMAGEN-FU2 ( $n=415$ ), we replicated CHIMGEN findings. The uncorrected statistical correlation map of UrbanSat with brain GMV in CHIMGEN showed significant spatial correlation with that of IMAGEN-FU2 ( $r=0.40$ ,  $P<0.001$ ; Extended Data Fig. 4). UrbanSat was correlated with GMVs of the mPFC ( $\rho=-0.15$ ,  $P=0.003$ ) and cerebellum ( $\rho=0.13$ ,  $P=0.009$ ), and SA of the mPFC

( $\rho=-0.19$ ,  $P<0.001$ ), but not CT of the mPFC ( $\rho=-0.03$ ,  $P=0.589$ ) (Fig. 3b and Supplementary Table 12). In voxel-wise analyses, we validated the negative correlation of UrbanSat with mPFC volume and positive correlation with cerebellar volume (Extended Data Fig. 4), both driven by NL and built-up% (Extended Data Fig. 5).

To exclude possible scanner and site effects, we performed separate analyses for each acquisition site of CHIMGEN and IMAGEN-FU2, carrying out a meta-analysis with an inverse

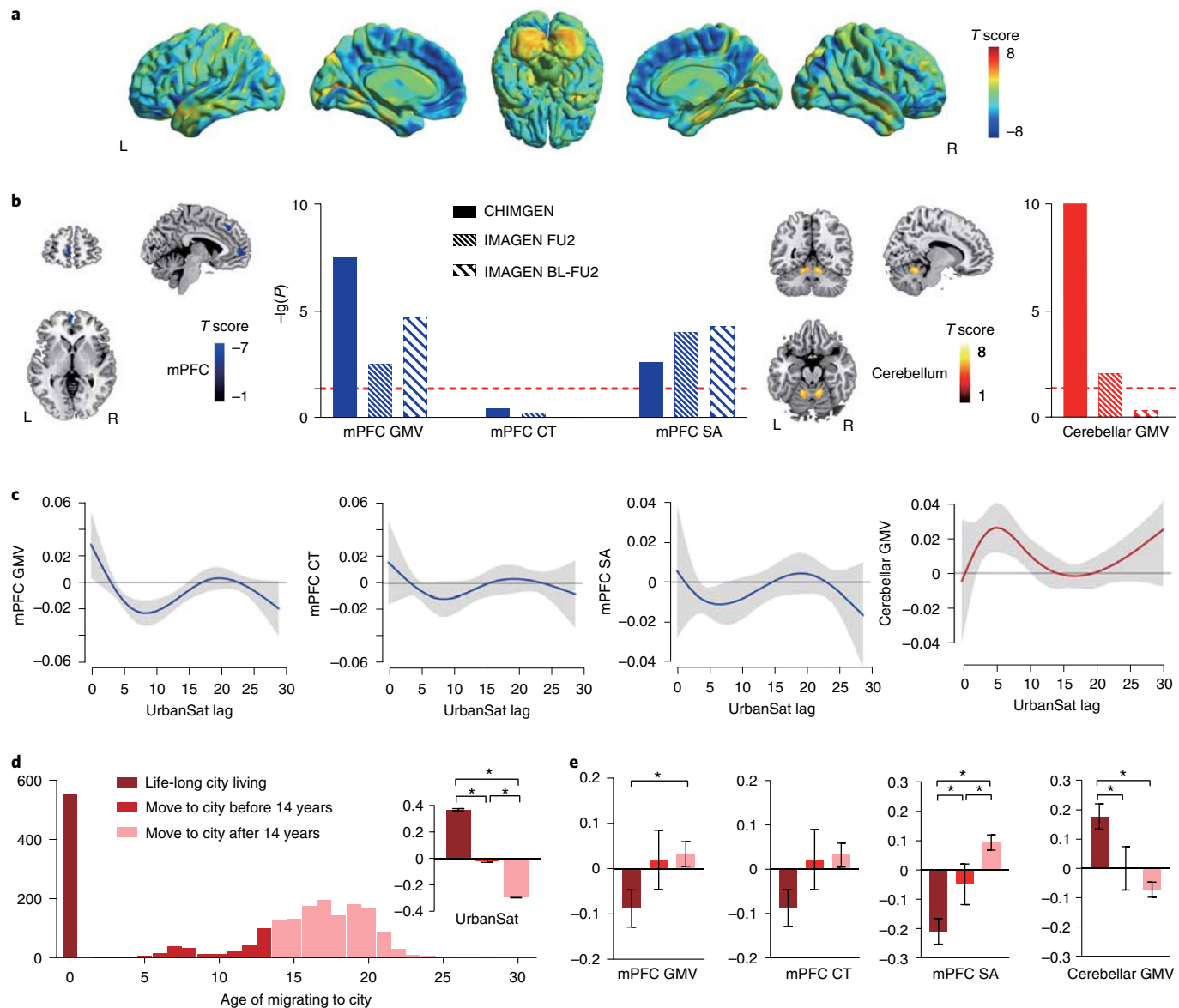


**Fig. 3 | Correlations of UrbanSat with brain structure.** **a**, Uncorrected statistical maps in the voxel-wise multiple regression of mean UrbanSat before 18 years with brain GMV under parametric testing in CHIMGEN ( $n=2,176$ ). **b**, In CHIMGEN, UrbanSat is negatively (blue) correlated with mPFC-GMV (left) and positively correlated with cerebellar-GMV (right) (FWE  $P_c < 0.05$ ). The correlation of UrbanSat with mPFC-GMV is driven by SA rather than CT, and these correlations are replicated in IMAGEN-FU2 ( $n=415$ ); UrbanSat is correlated with brain volumetric change in mPFC ( $n=340$ ) in IMAGEN BL-FU2, which is driven by the change of SA rather than CT ( $n=325$ ). Dashed red lines indicate the threshold of  $P = 0.05$ . **c**, Susceptibility period analysis of brain structure using DLM. In CHIMGEN, we observed a negative association of UrbanSat with mPFC-GMV during childhood and adolescence (age 4–15 years) and mPFC-SA during childhood (age 5–7 years) as well as a positive association with cerebellar-GMV during childhood (age 1–10 years). The y axis represents the changes of brain structural features associated with an increase of interquartile range of UrbanSat; the x axis is UrbanSat lag in years of ages. Grey areas indicate 95% CI. A susceptibility window is identified for the ages where the estimated 95% CI (shaded area) does not include zero. **d**, Numbers of participants migrating to city at different ages. Inset, UrbanSat is highest in participants with life-long city living ( $n=562$ ), medium in participants moving to city before 14 years ( $n=229$ ) and lowest in participants moving to city after 14 years ( $n=1,385$ ). **e**, Participants who were born in the city or migrated to an urban environment at an earlier age showed smaller mPFC-GMV and mPFC-SA as well as greater cerebellar-GMV than those with later exposure. Error bars show mean and s.e.m. BL, IMAGEN baseline assessment acquired at 14 years old; BL-FU2, IMAGEN BL-FU2 measures brain structural changes rate between BL of 14 years and FU2 of 19 years; CT, cortical thickness; DLM, distributed lag model; FU2, IMAGEN second follow-up assessment acquired at 19 years old; L, left; R, right; SA, surface area. \* $P < 0.05$ .

variance-weighted random-effects model (Methods and Supplementary Methods). UrbanSat remained significantly negatively correlated with mPFC-GMV and SA, and positively correlated with cerebellar-GMV (Extended Data Fig. 6 and Supplementary Table 13). Heterogeneity of effect sizes was low to moderate for all regions ( $I^2$  range 0.05–60.21%; Supplementary Table 13). Thus,

the observed correlation between UrbanSat and brain structure is robust across geographies and socio-cultural conditions.

We applied distributed lag models (DLMs) to identify susceptibility periods of lifetime UrbanSat on GMV and SA (Methods). We observed a negative association of UrbanSat with mPFC-GMV from age 4 to 15 years (Fig. 3c) and SA from age 5 to 7 years

(Fig. 3c), indicating a susceptibility period during childhood and adolescence, driven by NL, built-up%, cropland% and NDVI (Extended Data Fig. 7). Correlation of UrbanSat with cerebellar-GMV was significant from age 1 to 10 years, indicating a susceptibility period during childhood (Fig. 3c), driven by NL, built-up% and cropland% (Extended Data Fig. 7).

To investigate the relation between UrbanSat and brain development, we used the longitudinal IMAGEN dataset to calculate volumetric ( $n=340$ ) and SA/CT change rate per year ( $n=325$ ) between baseline (BL) at 14 and FU2 at 19 years (IMAGEN BL-FU2). Consistent with the susceptibility periods identified, UrbanSat was significantly correlated with brain volumetric development in the mPFC-ROI ( $\rho=0.24$ ,  $P<0.001$ ) but not cerebellum-ROI ( $\rho=-0.04$ ,  $P=0.456$ ). This correlation was driven by mPFC-SA changes ( $\rho=0.23$ ,  $P<0.001$ ), not by CT changes ( $\rho=0.002$ ,  $P=0.967$ ) (Supplementary Table 12).

To measure the relation between age of migration and brain structure, we split CHIMGEN participants into those who migrated to the city before age 14 years ( $n=229$ , mean age at migration  $8.24 \pm 4.86$  years), after age 14 years ( $n=1,385$ , mean age at migration  $17.17 \pm 2.68$  years) and life-long city-dwellers ( $n=562$ ) (Fig. 3d). We found that participants born in the city or early migrants showed smaller mPFC-GMV ( $P=0.032$ ) and SA ( $P<0.001$ ) as well as greater cerebellar-GMV ( $P<0.001$ ) than those with later exposure (Fig. 3e and Supplementary Table 14).

**No correlation of UrbanSat with white matter microstructure.** Using tract-based spatial statistics (TBSS) analysis of diffusion tensor imaging (DTI) data, we did not find significant correlation of UrbanSat with brain fractional anisotropy (FA) in either CHIMGEN or IMAGEN-FU2 (TFCE-FWE,  $P_c<0.05$ ).

**Correlations of UrbanSat with resting-state functional network connectivity.** Using group-independent component analysis of estimated 30 independent components (Supplementary Methods), we identified 17 resting-state networks (RSNs) related to cognitive and sensory-motor processes<sup>13</sup> in both CHIMGEN and IMAGEN ( $n=2,156$ ) (Extended Data Fig. 8). For each RSN, we tested the relation between mean UrbanSat and within-network functional connectivity (WNFC). A voxel-wise multiple regression analysis controlling for all confounders revealed a negative correlation of UrbanSat with WNFC in the mPFC of the anterior default mode network (aDMN) (peak MNI coordinate:  $x=-3$ ,  $y=69$ ,  $z=0$ ; 142 voxels; peak  $t$  value  $-6.33$ ), and positive correlations in the cerebellar vermis of the cerebellar network (CN) (peak MNI coordinate:  $x=-15$ ,  $y=-63$ ,  $z=-15$ ; 156 voxels; peak  $t$  value  $7.09$ ), in the left lingual gyrus (LG) of the medial visual network (mVN) (peak MNI coordinate:  $x=-12$ ,  $y=-90$ ,  $z=0$ ; 114 voxels; peak  $t$  value  $6.98$ ) and in the left LG of the lateral visual network (lVN) (peak MNI coordinate:  $x=-24$ ,  $y=-81$ ,  $z=-13$ ; 141 voxels; peak  $t$  value  $6.97$ ) (FWE  $P_c<0.05$ , additionally corrected for 17 RSNs; Methods) (Fig. 4a). Voxel-based correlations of individual satellite measures with WNFCs of each RSN are shown in Extended Data Fig. 9. The correlations of UrbanSat with WNFCs in CHIMGEN were replicated in ROI-based analyses in IMAGEN-FU2 ( $n=351$ ) (aDMN:  $\rho=-0.18$ ,  $P<0.001$ ; CN:  $\rho=0.26$ ,  $P<0.001$ ; mVN:  $\rho=0.24$ ,  $P<0.001$ ; lVN:  $\rho=0.24$ ,  $P<0.001$ ) (Fig. 4b and Supplementary Table 12). Only the aDMN and CN results were replicated in voxel-wise analyses in IMAGEN-FU2 (Extended Data Fig. 9).

Among 136 BNFCs, UrbanSat was correlated with 49 BNFCs in CHIMGEN ( $P_c<0.05$ , 10,000 permutations; Methods) (Fig. 4e), four of which were replicated in IMAGEN-FU2 (Fig. 4f). These four BNFCs (aDMN-CN, aDMN-ECN, aDMN-rFPN and rFPN-lFPN) connect five brain functional networks (aDMN, CN, executive control network (ECN) and right or left frontoparietal network (r/lFPN)), implicated in self-referential thoughts<sup>14</sup> and executive control<sup>15</sup>.

The correlations of UrbanSat with WNFCs and BNFCs were stable in a meta-analysis of all CHIMGEN and IMAGEN sites (Extended Data Fig. 6 and Supplementary Table 13). Brain localization (Fig. 4b,f) and susceptibility periods (Fig. 4d,h) of WNFCs and BNFCs in CHIMGEN and IMAGEN were consistent with those observed for brain structure (Extended Data Figs. 7 and 9), except for non-significance during adolescence. The changes in WNFCs and BNFCs between 14 and 19 years in IMAGEN were correlated with UrbanSat (Fig. 4b,f, Supplementary Table 12 and Supplementary Results). In CHIMGEN, WNFCs and BNFCs were correlated with age of migration to the city (Fig. 4c,g and Supplementary Results).

**Correlations of UrbanSat with behaviour.** We investigated whether UrbanSat is related to measures of cognition and mental health, that is, depression and anxiety. In CHIMGEN ( $n=2,148$ ), the social cognition measure ‘perspective-taking’, perceiving a situation from an alternative point of view<sup>16</sup>, was positively correlated with UrbanSat (reaction time for perspective-taking:  $\rho=-0.16$ ,  $P_c<0.05$ , Bonferroni corrected for data categories and 21 behavioural assessments; Methods) and replicated in IMAGEN-FU2 ( $\rho=0.14$ ,  $P_c<0.05$ ) (Table 1, Extended Data Fig. 10 and Supplementary Table 15). A negative correlation between UrbanSat and reaction time for perspective-taking performance was observed from 12 to 22 years in CHIMGEN (Fig. 5a).

UrbanSat was correlated with depression symptoms assessed by Beck Depression Inventory (BDI) in CHIMGEN ( $n=2,170$ ) ( $\rho=0.15$ ,  $P_c<0.05$ ) (Table 1) with a susceptibility period from 3 to 12 years (Fig. 5a). As BDI was not available in IMAGEN, we validated this association using an instrument measuring core features of depression, the Rumination Scale Questionnaire (RSQ) ( $\rho=0.14$ ,  $P_c<0.05$ ) (Table 1 and Supplementary Methods).

In CHIMGEN and IMAGEN, increased NL and built-up% and decreased NDVI and cropland% were significantly correlated with enhanced perspective-taking performance and increased depression symptoms (Table 1). The susceptibility periods for individual satellite measures were similar to UrbanSat in CHIMGEN (Extended Data Fig. 7). Although most correlations of UrbanSat with brain and behaviour were consistent between males and females, some correlations, especially with brain development in IMAGEN BL-FU2, were sex specific (Supplementary Tables 16 and 17).

**Multiple mediation in UrbanSat-brain-behaviour.** We applied multiple mediation analysis to investigate whether the significant brain imaging measures mediate correlations of UrbanSat with perspective-taking and depression symptoms in CHIMGEN and IMAGEN-FU2 (Methods). In CHIMGEN, 9.15% of the correlation between UrbanSat and reaction time for perspective-taking was mediated by brain, namely mPFC-GMV (1.16%), the cerebellar-GMV (1.48%), WNFCs in aDMN (1.31%) and CN (1.52%), as well as by the BNFCs of aDMN-CN (1.07%), aDMN-ECN (2.15%) and aDMN-rFPN (1.95%) (Fig. 5b). Mediation was replicated in IMAGEN-FU2, with the association of UrbanSat with perspective-taking being mediated by mPFC-GMV (1.46%), WNFCs in aDMN (2.03%) and CN (0.92%) as well as BNFCs of aDMN-CN (1.62%) and aDMN-rFPN (1.20%) (Fig. 5b). There was no mediation of cerebellar-GMV in IMAGEN-FU2 (Supplementary Table 18).

In CHIMGEN, 9.68% of the correlation between UrbanSat and BDI was mediated by brain, namely mPFC-GMV (2.21%) and SA (0.80%), cerebellar-GMV (3.42%), WNFCs in aDMN (1.17%) and mVN (1.03%) and BNFC of aDMN-ECN (1.90%) (Fig. 5c). In IMAGEN-FU2, the correlation between UrbanSat and rumination was mediated by mPFC-GMV (1.89%), WNFC in aDMN (1.02%) and BNFC of aDMN-ECN (1.26%) (Fig. 5c), but not by cerebellar-GMV (Supplementary Table 18).

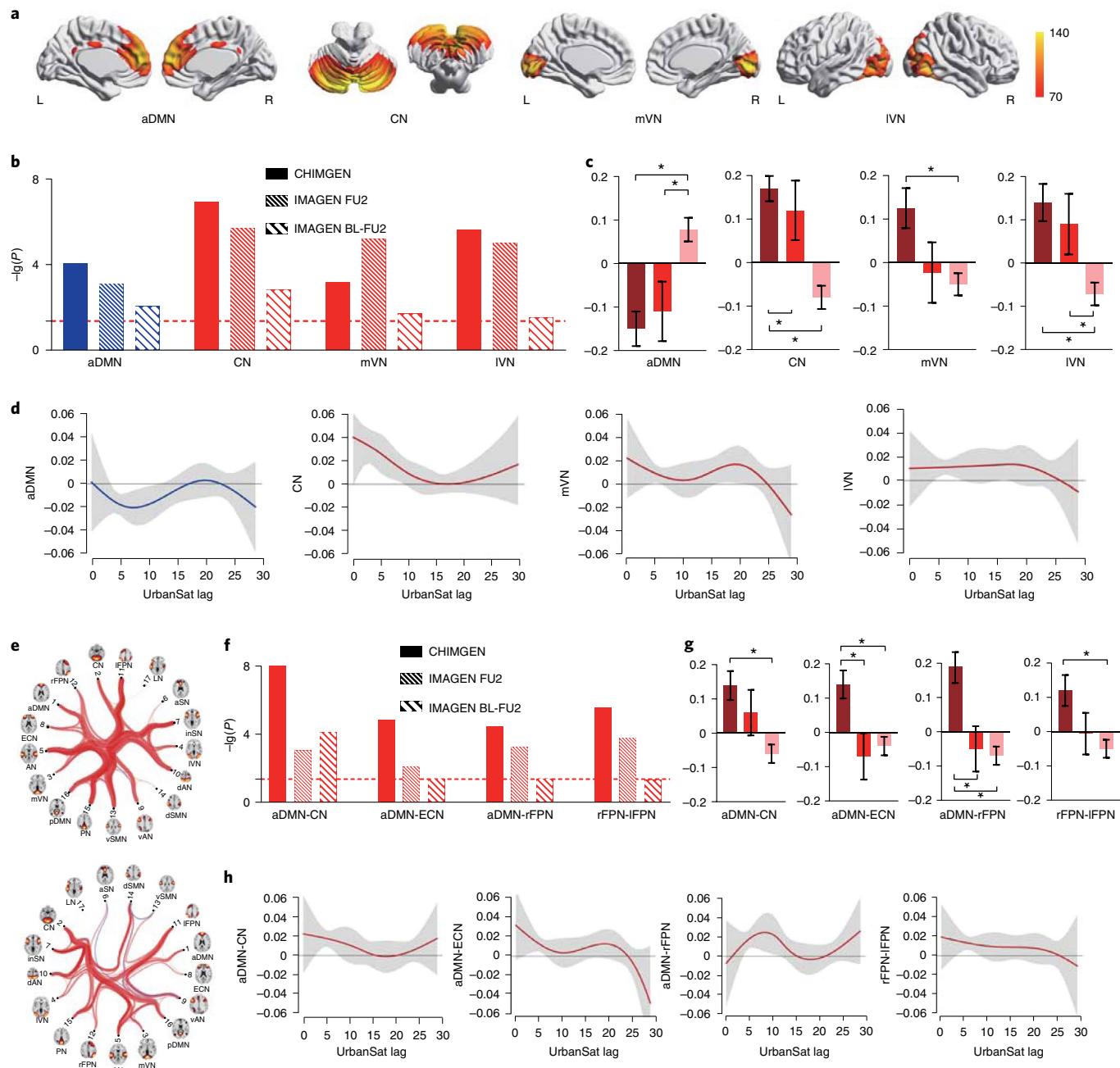


**Fig. 4 | Correlations of UrbanSat with WNFC and BNFC.** **a**, Voxel-wise multiple regression analysis controlling for confounders identified four WNFCs (aDMN, CN, mVN and IVN) correlated with mean UrbanSat before 18 years in CHIMGEN ( $n=2,156$ ). **b**, UrbanSat is negatively (blue) correlated with WNFC in mPFC of aDMN and positively correlated (red) with WNFC in CV of CN and left LG of mVN and IVN (FWE  $P_c < 0.05$ ). These correlations are replicated in IMAGEN-FU2 ( $n=351$ ). UrbanSat is correlated with change in these four WNFCs between 14 and 19 years in IMAGEN ( $n=83$ ). **c**, Life-long city-dwellers ( $n=559$ ) and earlier migrants ( $n=222$ ) showed greater WNFCs in CN, mVN and IVN but smaller WNFC in aDMN than later migrants ( $n=1,375$ ).

**d**, Susceptibility period analysis of WNFCs using DLM. In CHIMGEN, we observed significant negative association of UrbanSat with WNFC in aDMN during childhood and adolescence (age 4–12 years), positive association with WNFC in CN during childhood (ages 0–9 years) and with WNFC in IVN during childhood (age 5–9 years). No significant susceptibility periods are observed in the association of UrbanSat with WNFC in mVN. **e**, There are 49 BNFCs correlating with UrbanSat and 45 BNFCs correlating with NL in CHIMGEN ( $P_c < 0.05$ , 10,000 permutations). **f**, Correlations of UrbanSat with BNFCs of aDMN-CN, aDMN-ECN, aDMN-rFPN and rFPN-IFPN are replicated in IMAGEN-FU2; UrbanSat is also correlated with change in these four BNFCs between 14 and 19 years in IMAGEN BL-FU2. **g**, Life-long city-dwellers and earlier migrants showed greater BNFCs than later migrants. Error bars show mean and s.e.m. **h**, Susceptibility period analysis of BNFCs using DLM. In CHIMGEN, we observed significant positive association of UrbanSat with BNFCs of aDMN-CN (age 3–7 years), aDMN-ECN (age 3–6 years), aDMN-rFPN (age 4–10 years) and rFPN-IFPN (age 4–9 years) during childhood periods. L, left; R, right.

## Discussion

Using UrbanSat, a remote-sensing satellite measure, we characterized the relation of population density, a proxy of urbanicity, with

brain structure, function and behaviour during childhood and adolescence in large datasets in China and Europe. We provide converging evidence for association of UrbanSat during childhood and

**Table 1 | Correlations of UrbanSat and individual satellite measures with behaviour in CHIMGEN and IMAGEN**

Item	Statistics <sup>a</sup>	UrbanSat <sup>b</sup>	NL	Built-up%	Cropland%	NDVI
<b>CHIMGEN</b>						
<b>PT and Ag (n = 2,148)</b>						
ACC <sub>pt</sub>	0.21 (0.38)	0.061 (−0.04)	0.043 (−0.04)	0.141 (−0.03)	0.188 (0.03)	0.027 (0.05)
ACC <sub>agency</sub>	1.00 × 10 <sup>−9</sup> (0.21)	0.788 (−0.01)	0.568 (−0.01)	0.677 (−0.01)	0.948 (−0.001)	0.826 (0.01)
RT <sub>pt</sub> (ms)	1160.67 (740.39)	<b>&lt;0.001 (−0.16)</b>	<b>&lt;0.001 (−0.14)</b>	<b>&lt;0.001 (−0.13)</b>	<b>&lt;0.001 (0.14)</b>	<b>&lt;0.001 (0.13)</b>
RT <sub>agency</sub> (ms)	−7.44 (363.22)	0.618 (0.01)	0.336 (0.02)	0.369 (0.02)	0.854 (−0.004)	0.122 (−0.03)
<b>Mental health (n = 2170)</b>						
BDI	2.00 (5.00)	<b>&lt;0.001 (0.15)</b>	<b>&lt;0.001 (0.16)</b>	<b>&lt;0.001 (0.11)</b>	<b>&lt;0.001 (−0.14)</b>	<b>&lt;0.001 (−0.10)</b>
SA	30.00 (9.00)	0.637 (0.01)	0.548 (0.01)	0.418 (−0.02)	0.383 (−0.02)	0.690 (−0.01)
TA	33.00 (9.00)	0.250 (0.02)	0.085 (0.04)	0.832 (0.01)	0.218 (−0.03)	0.309 (−0.02)
<b>IMAGEN-FU2</b>						
<b>PT</b>						
IRI (n = 342)	19.00 (5.00)	<b>0.009 (0.14)</b>	0.565 (0.03)	<b>0.008 (0.15)</b>	0.085 (−0.10)	0.879 (−0.01)
<b>Mental health</b>						
RSQ (n = 346)	35.00 (15.00)	<b>0.009 (0.14)</b>	0.431 (0.04)	<b>0.002 (0.17)</b>	0.926 (−0.01)	0.653 (0.02)
DAWBA-GA (n = 447) (Y/N)	355/92	0.451 (−0.22)	0.914 (0.001)	0.901 (0.06)	0.319 (−0.55)	0.513 (−3.35 × 10 <sup>−4</sup> )
CIDI-AS (n = 391)	6.00 (10.00)	0.196 (0.07)	0.559 (0.03)	0.202 (0.07)	0.339 (−0.05)	0.588 (−0.03)

ACC, accuracy; Ag, agency performance; BDI, Beck Depression Index; CIDI-AS, Anxiety Screening from the Composite International Diagnostic Interview; DAWBA-GA, Generalized Anxiety Scale from The Development and Well-Being Assessment Interview; IRI, Interpersonal Reactivity Index; PT, perspective-taking; RSQ, ruminating scale questionnaire; RT, reaction time; SA, state anxiety; TA, trait anxiety.

<sup>a</sup>Statistics are shown as median (quantile interval). <sup>b</sup>Spearman correlations are used to test the correlations between individual satellite measures and behaviours (except for DAWBA-GA) controlling for confounding covariates, which is shown as correlation P value ( $\rho$  value). In the DAWBA-GA, logistic regression is used to test the correlations between individual satellite measures and anxiety, which is shown as P value ( $P$  value). In CHIMGEN, the significant results after Bonferroni  $P_c < 0.05$  (uncorrected  $P < 0.05/5 = 0.01$ ) are shown in bold; in IMAGEN, the significant results after Bonferroni  $P_c < 0.05$  (uncorrected  $P < 0.05/5 = 0.01$ ) are shown in bold.

adolescence with GMV and SA of mPFC as well as WNFCs and BNFCs of aDMN. No significant association was observed with CT and FA. mPFC and aDMN mediate the correlation between UrbanSat and improved perspective-taking and increased depression symptoms. We also found positive correlations of UrbanSat during childhood with cerebellar volume, which mediated the association with perspective-taking and depression symptoms. We extend previous observations reporting an association of depression symptoms with urban settings<sup>17</sup> by demonstrating the stability of this observation in different geographical and sociocultural regions, and by discovering possible underlying brain mechanisms and susceptibility periods during childhood and adolescent development.

Our results suggest that urban living has both beneficial and adverse correlations with health: enhanced social cognition (perspective-taking) and increased depression symptoms, in contrast to previous studies, which mainly reported adverse aspects of urbanicity<sup>18</sup>. The mPFC, the core brain area of the aDMN, has been implicated in a variety of social cognition and affective functions commonly compromised in psychiatric disorders<sup>19</sup>. The susceptibility of mPFC to urban environment is supported by the greater sensitivity of mPFC to urbanicity-related risk factors including chronic stress<sup>20</sup> and air pollution<sup>21</sup>. While our findings are consistent with reports of an association between urbanicity and mPFC in smaller European samples<sup>22</sup>, they differ from these studies as we found associations with GMV and SA rather than CT, and an absence of sex specificity.

We found a positive correlation of UrbanSat with cerebellar volume, a mediator for the association of UrbanSat with perspective-taking and depression symptoms. The functional network connectivity of the cerebellum also mediates the association of UrbanSat with perspective-taking. Cerebellar lesions cause the cerebellar cognitive affective syndrome, characterized by impairments

in executive function and memory, as well as affect<sup>23</sup>. Animal studies extend these findings to stress-dependent depressive affect<sup>24</sup> and impairment in social behaviour<sup>25</sup>. It is tempting to speculate that these pathways may connect to brain regions involved in perspective-taking and depression symptoms<sup>26</sup>. Imaging features related to cerebellum showed susceptibility periods to high population density at age 1–10 years, during which cerebellum and cortex are increasing in volume<sup>27–29</sup>.

While previous studies focused on the effect of mean exposure to urban living on brain and mental health<sup>30</sup>, we identified neurodevelopmental periods with increased susceptibility to urban living. Consistent with observations of susceptibility periods of non-affective psychosis to residential mobility during childhood and adolescence<sup>31</sup>, we found that structure and function of mPFC, as well as depression symptoms, have pronounced susceptibility to high population density during childhood and adolescence, a period more sensitive to social stress<sup>32</sup>. Perspective-taking was more sensitive to high population density during adolescence and young adulthood, implying a time window for neurobehavioural interventions targeting social cognition.

Our results are suggestive of a cumulative relation of urbanicity with brain and behaviour, whereby participants born or migrating to the city at an earlier age had more pronounced effects than those who become city-dwellers later. Given that CHIMGEN participants were students who moved to cities for their studies, we do not have any data on people who, after spending some years in the city, moved back to the countryside. We also do not have data to distinguish possible short but extreme exposure to urban life, in utero or during susceptibility periods from moderate continuous exposure.

We found several shared relations of high population density in urban settings with brain structure and function as well as on social cognition and mental health in both CHIMGEN and IMAGEN,

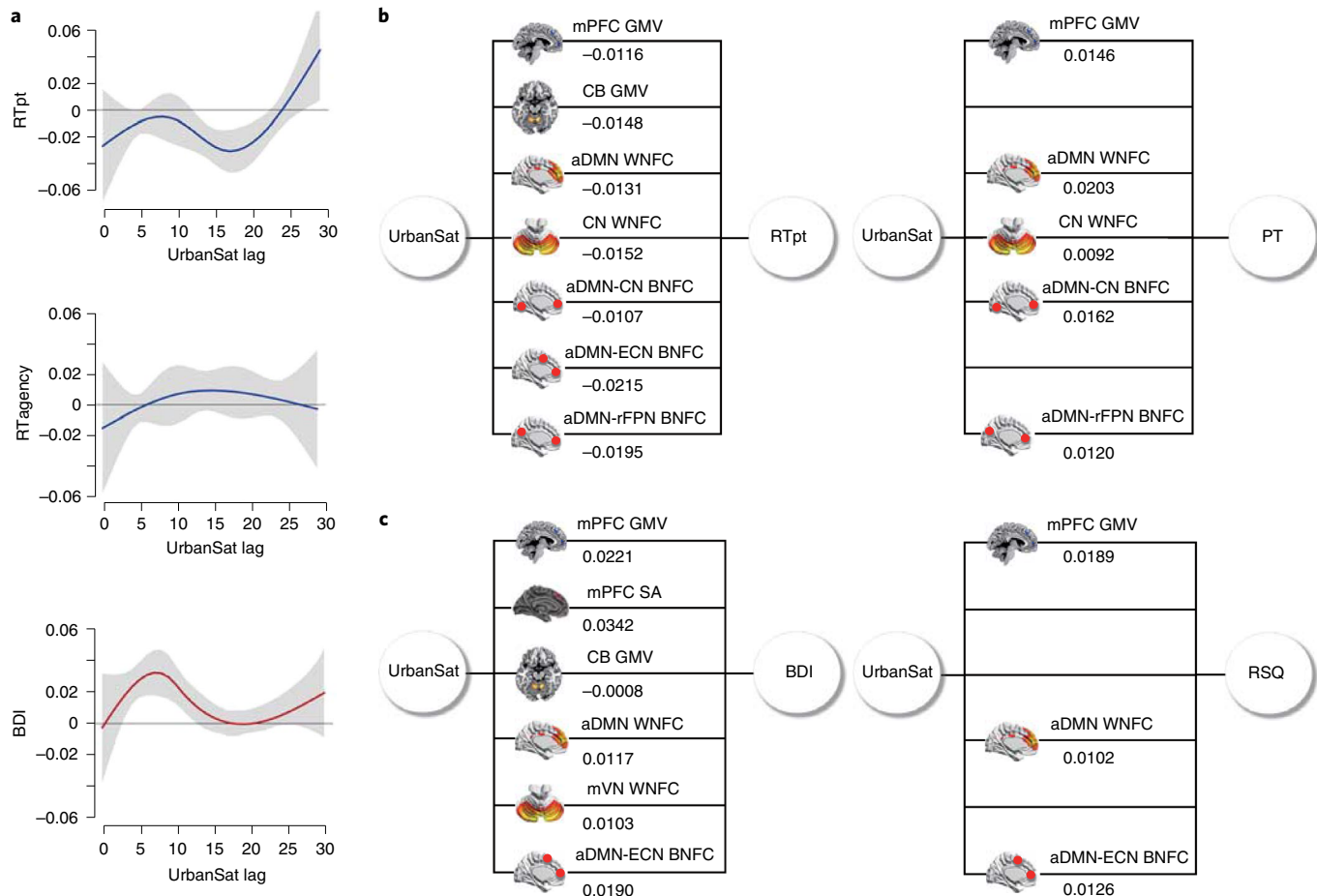


**Fig. 5 | Susceptibility periods of behaviour using DLM and multiple mediation of UrbanSat-brain-behaviour.** **a**, UrbanSat is negatively correlated with reaction time for perspective-taking (top) from age 12 to 22 years but not with that for agency (medium) in CHIMGEN ( $n=2,148$ ). UrbanSat is positively correlated with depression symptoms (BDI) from age 3 to 12 years in CHIMGEN ( $n=2,170$ ) (bottom). **b**, In CHIMGEN, the correlation of UrbanSat with perspective-taking performance is mediated by mPFC and cerebellar-GMV, WNFCs in aDMN and CN, as well as BNFCs of aDMN-CN, aDMN-ECN and aDMN-rFPN (left); These mediation effects are replicated in IMAGEN-FU2 except for cerebellar-GMV and BNFC of aDMN-ECN (right). **c**, In CHIMGEN, the correlation between UrbanSat and BDI is mediated by mPFC-GMV and SA, cerebellar-GMV, WNFCs in aDMN and mVN as well as BNFC of aDMN-ECN (left); The mediation effects of the mPFC-GMV, WNFC in aDMN and BNFC of aDMN-ECN are replicated in IMAGEN-FU2 (right). PT, perspective-taking measured by interpersonal reactivity index (IRI); RSQ, Ruminating Scale Questionnaire; RT<sub>pt</sub> and RT<sub>agency</sub>, reaction time for perspective-taking and agency.

indicating their generalization to other sociocultural conditions and geographies. The relation of urban living with brain development during adolescence was confirmed by exploring the correlation of UrbanSat with brain structural and functional changes from age 14 to 19 years in IMAGEN. Taking into account normative references<sup>27–29</sup>, our observations are consistent with an accelerated development in densely populated urban areas of cerebellum during childhood and mPFC during childhood and adolescence. We also found inconsistent results between CHIMGEN and IMAGEN: only 4 of 49 BNFCs correlating with UrbanSat in CHIMGEN were replicated in IMAGEN. The more extensive relations of urban living with BNFCs in CHIMGEN may reflect the more drastic changes in urbanization in China compared with Europe<sup>6</sup>, but may also relate to confounding factors beyond the covariates controlled in our study<sup>33</sup>.

UrbanSat was correlated with GMV, SA and functional connectivity, but not with FA and CT, indicating different sensitivities of brain properties to residential environments. UrbanSat showed positive correlation with cerebellar volume, negative correlation with mPFC volume, but non-significant correlation with volumes of other regions, suggesting different spatial sensitivities to residential environments. The cerebellum was sensitive to urban residential

environments during childhood, whereas the mPFC was sensitive during both childhood and adolescence, indicating different temporal sensitivities to residential environments. This framework of different spatial and temporal sensitivities to urban residential environments may help to understand the association of urban living with brain and mental health.

High population density, a general measure of urbanicity, can cause increased social stress and air pollution, both of which affect brain structure in young people<sup>34,35</sup>. A recent study observed an association of urbanicity with brain activity in regions linked to social stress processing<sup>30</sup>. Such brain changes may mediate the well-established relation of urbanicity with mental health, including mood disorders<sup>36</sup> and social cognition<sup>18</sup>. Stress in childhood can accelerate brain development and lead to faster maturation of certain brain regions during adolescence, including cerebellum and mPFC<sup>37</sup>. Faster brain maturation results in enhanced cognitive development<sup>38</sup> and may account in part for the positive correlation of urbanicity and perspective-taking observed in our study. However, faster maturation of mPFC and cerebellum may come at a cost of decreased plasticity, including of fear extinction mechanisms (mPFC), which may contribute to increased vulnerability to

anxiety and depression<sup>39</sup>. Air pollution induces neuroinflammation in the brain, leading to damage and loss of neural tissue in prefrontal cortex<sup>35</sup>, and may provoke depression symptoms<sup>40</sup>. Thus, urban upbringing may cause affective and anxiety symptoms by way of both increased social stress and pollution.

Remotely sensed satellite data play a critical role in monitoring the Earth's surface to track environmental conditions that are intimately related to human health<sup>10</sup>. Satellite data are applied to map urbanization, poverty, climate change and pollution, as well as the spread of infectious diseases<sup>10</sup>. Our study extends the application of remote-sensing satellite data and provides a method to characterize and monitor spatial and temporal patterns of risk for mental disorders. In the optimized CFA models, the four satellite measures contributing to UrbanSat showed different factor loadings. NL with the highest factor loading can capture the physical environmental features of urbanicity, such as patterns of human settlements<sup>41</sup>, urban expansion<sup>42</sup> and population counts<sup>43</sup>, as well as information about social-environmental features of urbanicity, such as economic activity<sup>44</sup>. Built-up% and cropland% with medium factor loadings mainly reflect physical-environmental features of urbanicity. NDVI with the smallest factor loading measures residential greenness and has been used extensively to record the distribution of green spaces in urban settings<sup>45</sup>. UrbanSat mainly reflects the physical-environmental features and indicates the social-environmental features of urbanicity only indirectly.

For privacy reasons, our satellite measures were obfuscated to a spatial resolution of 1 km, preventing the capture of important aspects of urban life, such as daily mobility paths. Future studies will investigate the integrated effect of urban physical and social environment, and their interaction with genetics and relation to brain and behaviour. MICE is a flexible tool for multiple imputation of missing data, which properly accounts for uncertainty in the downstream estimates by combining subsequent estimates from different imputed datasets. This approach also accommodates the multiple training-test splits of the dataset to ensure that the estimates of generalizability we obtain are unbiased throughout the imputation. The disadvantage of MICE is the difficulty in combining multiple imputed datasets with voxel-wise neuroimaging statistics. Although several sensitivity analyses were applied after the multiple imputation and led to identical conclusions, we are still not in a position to fully exclude the potential bias derived from missing data. This study is not epidemiological but neurobiological, aiming to identify brain mechanisms by which urbanicity influences behaviour. How representative the identified mechanisms are among the general population is a different task, for future epidemiological studies.

Our findings were made possible due to recent advancements in remote-sensing satellite technologies which were leveraged to measure the relation of urbanicity with brain and behaviour. We were able to (1) apply a general measure of urbanicity, that is, population density, which is not dependent on census definitions of urban areas that might be conflated by densely populated rural areas or sparsely populated areas within urban settlements, or that may vary between nations;<sup>5</sup> (2) obtain a high spatial and temporal resolution;<sup>10</sup> (3) use a measure applicable anywhere on Earth from the 1970s to the present day. Thus, UrbanSat provides a unique opportunity to identify the cumulative effects and susceptibility periods of urbanicity on brain and behaviour. However, we note that UrbanSat cannot unravel environmental pathways and their interactions that cause the aversive effects of urban living. This is a task for subsequent studies with access to sufficient ground-level data for comprehensive characterization of causal environmental pathways that underlie the observed correlations.

In the current work, we provide proof of principle establishing the use of satellite data to inform the relation between urban environment, brain and behaviour. As our approach can be extended and generalized to other geographies and is easy to implement even in the

absence of detailed or directly comparable ground-level data, it may be relevant for public health, policy and urban planning globally.

## Methods

**Ethical approval.** The Chinese Imaging Genetics (CHIMGEN) project was approved by the ethics committee of 31 centres in China<sup>1</sup>, and written informed consent was obtained from each participant<sup>11</sup>. The IMAGEN study was approved by local research ethics committees at each research site. Informed consent was sought from all participants and a parent or guardian of each participant<sup>12</sup>.

**Participants.** The CHIMGEN project collected genetic, transcriptomic, environmental, neuroimaging and behavioural data of 7,306 healthy Chinese Han participants aged 18–30 years recruited from 31 centres of 21 cities in Mainland China<sup>1</sup>. At the time of data analysis (January 2018), data were available for 5,425 participants. The IMAGEN project is the first European multisite and longitudinal study<sup>13</sup>, and comprehensive genetic, transcriptomic, epigenetic, environmental, neuroimaging and neurocognitive data were collected from more than 2,000 14-year-old adolescents in 2009. Brain imaging measures were longitudinally assessed at age 14 years (baseline, BL) and 19 years (second follow-up, FU2). Most of the neurocognitive and mental health outcomes were longitudinally assessed at BL, FU1 (16 years) and FU2. The approach for sample selection in CHIMGEN and IMAGEN is described in the Supplementary Methods and is shown in Extended Data Fig. 1.

**Data collection. Residential geographies.** For each CHIMGEN participant who had consented to provide residential information, we recorded the precise residential addresses in each year from birth to recruitment and the category of each place (1 for rural, 2 for town or 3 for city) as determined according to the National Bureau of Statistics of China (Supplementary Methods). However, since residential histories were not obtained prospectively, we were not in a position to fully exclude the possibility of recall bias. Finally, 3,336 participants who provided their lifetime residential geographies were included in the further analysis. The remaining 2,089 participants were excluded because they only provided their residential addresses at the time point of recruitment but refused to provide their residential addresses at any other time points since birth.

At the time of the second follow-up, 561 IMAGEN participants provided their precise residential addresses for each year from birth to recruitment and the category of each place (1 for rural, 2 for town or 3 for city) (Supplementary Methods). To protect the anonymity of participants in CHIMGEN and IMAGEN, these addresses have been obfuscated to 1 km scaled longitude and latitude based on the Google Earth Engine (GEE) coordinate system using code (<https://github.com/crickfan/geo-anonymization>).

**Remote-sensing satellite data.** GHSL<sup>9</sup>, NL<sup>46</sup>, NDVI<sup>47</sup>, NDBI<sup>48</sup>, NDWI<sup>49</sup> and GLCM<sup>50</sup> were extracted from GEE and the European Space Agency platform to measure different urban characteristics based on the acquired lifetime individual geographies (Supplementary Methods and Supplementary Tables 7 and 24). There are 22 indicators in GLCM, which belong to 9 land cover types: cropland%, forest%, grassland%, shrubland%, bareland%, snow%, ice%, water body% and built-up%<sup>51,52</sup>. Among the 3,336 participants from CHIMGEN, we successfully extracted satellite measures from 3,306 participants. The other 30 participants were excluded because extraction of satellite measures failed in more than three years. In the present study, only land cover types with mean percentage above 1% before 18 years of participants from CHIMGEN ( $n=3,306$ ) and IMAGEN-FU2 ( $n=561$ ) were included in further analysis, including the land cover types of cropland% (CHIMGEN, 64.21%; IMAGEN, 13.65%), forest% (CHIMGEN, 5.00%; IMAGEN, 7.31%), grassland% (CHIMGEN, 3.01%; IMAGEN, 7.54%), water body% (CHIMGEN, 3.81%; IMAGEN, 1.37%) and built-up% (CHIMGEN, 29.14%; IMAGEN, 67.03%). Finally, nine satellite-based measures of urbanicity (NL, NDVI, NDBI, NDWI, cropland%, forest%, grassland%, water body% and built-up%) from CHIMGEN ( $n=3,306$ ) and IMAGEN-FU2 ( $n=561$ ) were included in further analysis.

**Confounding covariates data.** In CHIMGEN and IMAGEN, we controlled for age, gender, education, site, BMI, genetic population stratification, total intracranial volume, mean corticale thickness, total surface area and SES in the correlation of satellite-based measure of urbanicity with brain and behaviour. Parental history of mental illness was an exclusion criterion for CHIMGEN, but not in IMAGEN, where this variable was controlled for in IMAGEN data analyses (Supplementary Methods).

**Neuroimaging data.** Among participants with lifetime satellite measures and confounding covariates, 2,176 participants from CHIMGEN and 482 participants from IMAGEN-FU2 with at least one modality of neuroimaging data were included in the analysis. T1-weighted imaging, DTI and resting-state functional imaging were acquired using 3.0-T MRI scanners from 28 sites of CHIMGEN and 6 sites of IMAGEN-FU2 (Supplementary Tables 19–23). Brain GMV, CT and SA were calculated from the T1-weighted imaging, FA from the DTI, as well as WNFC and BNFC from the resting-state functional MRI. The detailed preprocessing and calculation methods are described in Supplementary Methods and

<http://chimgen.tmu.edu.cn/en/index.php?c=article&id=2034>. Finally, in CHIMGEN, qualified GMV data were available in 2,176 participants, CT and SA data in 2,164 participants, FA of TBSS data in 2,158 participants as well as WNFC and BNFC data in 2,156 participants.

In IMAGEN, among the remaining 482 participants, 415 (FU2) were included in GMV analysis, 420 (FU2) in CT and SA analysis, 436 (FU2) in TBSS analysis and 351 (FU2) in WNFC and BNFC analyses (Supplementary Methods). For the 340 participants with qualified structural imaging data at both BL (14 years) and FU2 (19 years) in IMAGEN, structural imaging data were pre-processed using the pairwise longitudinal tool implemented in SPM12 for longitudinal voxel-based morphometry analysis<sup>53</sup>. Finally, we obtained year-averaged GMV change maps for 340 participants and year-averaged CT and SA change maps for 325 participants. In 83 participants with qualified fMRI data at both BL (14 years) and FU2 (19 years), we calculated WNFC and BNFC for each participant at each stage, then obtained the WNFC and BNFC change maps of the 83 participants (Supplementary Methods).

**Behavioural data.** Among the 2,176 participants with at least one type of qualified MRI data in CHIMGEN, 2,173 were finally included in the analysis of verbal learning memory, 2,063 in working memory, 2,139 in information processing speed, 2,148 in social cognition (Extended Data Fig. 10), 2,024 in cognitive control and 2,170 in depression and anxiety state of mental health assessment (Supplementary Methods).

Only statistically significant behavioural variables with UrbanSat would be validated in IMAGEN. Among the 482 participants, complete data on perspective-taking was available for 342 participants (FU2). Complete data were available for the RSQ in 346 participants (FU2), the Generalized Anxiety Scale from The Development and Well-Being Assessment Interview (DAWBA-GA) in 447 participants (FU2) and the Anxiety Screening for Composite International Diagnostic Interview (CIDI-DIA) in 391 participants (FU2) (Supplementary Methods).

**Statistical analysis. Demographic statistics.** We compared demographic characteristics between the final analytical sample ( $n = 2,176$  for CHIMGEN;  $n = 415$  for IMAGEN-FU2) and total sample ( $n = 5425$  for CHIMGEN;  $n = 1411$  for IMAGEN-FU2) using bias-corrected bootstrapping (Supplementary Methods). To test selection bias, we compared differences in demographic and behavioural variables between the included sample ( $n = 3,306$  for CHIMGEN;  $n = 561$  for IMAGEN-FU2) and the excluded sample ( $n = 2,119$  for CHIMGEN;  $n = 850$  for IMAGEN-FU2) using Wilcoxon rank sum test and chi-square analysis. While we found subtle but significant differences in a minority of variables that did not relate to the main behavioural results (perspective-taking and depressive symptoms) (Supplementary Tables 5 and 6), we cannot fully rule out an influence of selection bias on our findings. We controlled for demographic variables in the main analyses, including the significantly different variables age, gender, education, BMI and SES.

**UrbanSat calculation.** Tenfold cross-validation of multiple imputation for missing values. To calculate annual UrbanSat scores for each participant ( $n = 3,306$  for CHIMGEN) from birth to age of recruitment, we required satellite data from 1986 to 2018. However, the available satellite data did not cover the entire time period. For example, NL data were only available from 1992 to 2013 (Supplementary Table 7), indicating that 7,560 of 78,315 spatiotemporal points were missing (data missing rate 9.65%). Thus, we needed to impute the missing values for the nine satellite measures. The numbers of imputed years for each satellite-based measure and the number of CHIMGEN participants with missing data are presented in Supplementary Table 8. The imputation strategy is shown graphically in Extended Data Fig. 2.

We used MICE as implemented in the ‘mice’ R package<sup>54</sup> to impute the nine annual satellite registrations and generate ten complete datasets. The data were input as ‘wide’ format. The imputation models of predictorMatrix with default settings and predicted mean matching approach in the ‘mice’ R package were used in the multiple imputation process. We used 20 iterations of Gibbs sampling in the ‘mice’ R package.

Multiple training–test splits of the dataset were performed to ensure that the estimates of generalizability we obtain are unbiased throughout the analytic pipeline. Specifically, the nine satellite measures of 3,306 participants with missing data were randomly and equally divided into ten groups. Then, tenfold cross-validation was used to build the imputation diagnostic models in the training datasets and to predict missing values of satellite measures in the test datasets using MICE. For each fold, 90% of participants were used as a training dataset to build the imputation diagnostic model, then this diagnostic model was used to predict the missing values in the other 10% of participants in the test dataset. This process was applied in ten folds to predict all missing satellite data of 3,306 participants (Extended Data Fig. 2).

The IMAGEN participants born between 1994 and 1998 were recruited from 2009 to 2010 at baseline and followed up from 2015 to 2016. Thus, we have almost all true exposure values of the nine satellite measures for these participants. The only exception is the lack of NL data for 2014, 2015 and 2016. The same imputation methods were applied in these three years.

Tenfold cross-validation of CFA. NL, NDVI, NDBI, NDWI, cropland%, forest%, grassland%, water body% and built-up% have all been reported to measure urban environment (Supplementary Methods). As we hypothesize that each individual satellite-based measure contributes to the measurement of urban environment, we directly apply CFA but not exploratory factor analysis. The aim of CFA in this study is to construct a latent variable (UrbanSat) to comprehensively reflect urban environments, which was carried out using the R package ‘lavaan’ (<https://cran.r-project.org/web/packages/lavaan>)<sup>55</sup>. The same ten cross-validation splits as applied in the imputation process were used to optimize the CFA models and to predict annual UrbanSat scores of each participant from birth to age of recruitment. For each fold, 90% of participants were used to build the CFA model, and the optimized CFA model was used to calculate the UrbanSat scores for the other 10% of participants. For each fold, two criteria were used to optimize the CFA model by selecting appropriate satellite-based measures of urbanicity. The first criterion was the goodness of fit of the CFA model, which can be assessed by Tucker–Lewis index, comparative fit index, chi square, RMSEA and SRMR. The criteria for excellent model fit were TSI > 0.95, comparative fit index > 0.95, RMSEA < 0.06 and SRMR < 0.08 (refs. <sup>56–58</sup>). The second criterion was the inclusion of satellite-based measures as much as possible to better reflect different aspects of urbanicity. Specifically, in the first imputed satellite dataset, we initially constructed a CFA model by including all nine satellite-based measures of urbanicity in the training dataset of each fold. Based on the factor loadings of the nine satellite-based measures, we removed the satellite measure with the smallest factor loading and repeated the CFA modelling. These steps were iterated until the resulting CFA model satisfied our criteria for excellent model fit in the training dataset. The factor loadings of the optimized CFA model were used to calculate UrbanSat scores in the test dataset. This process was applied in ten folds to predict all out-of-sample lifetime UrbanSat scores of 3,306 participants. And the same process was applied from the first imputed satellite datasets to the tenth ones to generate ten datasets of lifetime UrbanSat scores of 3,306 participants (Extended Data Fig. 2).

The statistical estimate combination between voxel-wise neuroimaging analyses and the multiple imputed UrbanSat is not supported by the current version of Statistical Parametric Mapping (SPM12) software implemented in MATLAB R2018a (<http://www.fil.ion.ucl.ac.uk/spm>) during the model estimation. Therefore, we applied Rubin’s rules<sup>59</sup> to combine the ten datasets of UrbanSat scores derived from MICE imputation. The combined UrbanSat scores were related to the further voxel-wise whole brain analysis and susceptibility period analysis. Subsequently, we performed several sensitivity analyses as explained below.

**Sensitivity analysis.** The combined UrbanSat scores according to Rubin’s rules may underestimate the uncertainty in the downstream statistical estimates since they do not propagate uncertainty about the multiple imputation process. To test the potential uncertainty caused by the multiple imputation of satellite data, we combine this with multiple sensitivity analyses including the statistical comparison of subsequent mass-univariate voxel-wise neuroimaging analyses using multiple versions of the imputed UrbanSat and the estimation of ROI-level analyses where the multiple imputed UrbanSat were combined in a statistically principled fashion. Firstly, voxel-wise multiple regression analysis of each imputed UrbanSat with whole brain GMV adjusted for all confounding covariates in 2,176 participants was performed (FWE  $P_c < 0.05$ ). Secondly, the significant brain ROI was firstly identified from the voxel-wise multiple regression between the combined UrbanSat score following Rubin’s rules<sup>59</sup> and whole brain GMV after controlling confounding factors (FWE  $P_c < 0.05$ ). The ‘mice’ R package<sup>54</sup> was applied to pool the statistical estimates between ten imputed UrbanSat scores and brain ROI GMV value after controlling for confounding factors.

To test the potential bias caused by the imputation of satellite data, sensitivity analysis was additionally performed in participants with complete satellite and neuroimaging data. Among the 3,306 CHIMGEN participants with complete residential information, 1,460 participants had nine complete satellite measures from birth to age of recruitment and brain imaging data. This subset of participants was used to construct the out-of-sample CFA models and to calculate the annual UrbanSat scores before 18 years for each participant. Then the sensitivity analysis was performed to identify voxel-wise analysis between GMV and UrbanSat adjusted for all confounding covariates in 1,460 participants (FWE  $P_c < 0.05$ ).

In addition, the ‘mice’ R package<sup>54</sup> was also applied to pool the multiple statistical estimates between ten imputed datasets of UrbanSat scores and behaviours after controlling confounding factors.

**Correlation analyses of mean UrbanSat with brain imaging measures.** The voxel-wise multiple regression of mean UrbanSat before 18 years with brain GMV was performed in CHIMGEN ( $n = 2,176$ ) using Statistical Parametric Mapping (SPM12) implemented in MATLAB R2018a (<http://www.fil.ion.ucl.ac.uk/spm>) (Supplementary Methods). Statistical significance of the voxel-wise multiple regression models in relation to mean UrbanSat with neuroimaging data was assessed by parametric testing FWE correction, where we corrected for voxel numbers, six imaging features (GMV, CT, SA, FA, WNFC and BNFC) and two data types (neuroimaging and behavioural data). We therefore set a significance threshold of FWE-corrected  $P_c < 0.05$  (equal to an uncorrected  $P < (1.25 \times 10^{-6}/6/2) = 1.01 \times 10^{-7}$ ) in brain structure analysis in CHIMGEN.

The voxel-wise multiple regression model of UrbanSat with brain GMV adjusting for confounders was also performed using permutation-based non-parametric testing with TFCE with correcting for FWE (TFCE-FWE,  $P_c < 0.05$ ) as implemented in 'randomise' for FMRIB Software Library (FSL) v5.0 (<https://fsl.fmrib.ox.ac.uk/fsl/fslwiki/Randomise/UserGuide>). The more conservative results were used for the further ROI analysis.

For the voxel-wise BNFC analyses, we additionally corrected for the number of functional networks ( $n=17$ ), resulting in an FWE-corrected  $P_c < 0.05$  (uncorrected  $P < (1.25 \times 10^{-6}/6/17/2) = 6.13 \times 10^{-9}$ ). For the pairwise BNFC analyses, statistical significance of the partial correlation between UrbanSat and BNFC was assessed by permutation testing in reference to a prior study<sup>60</sup> (Supplementary Methods).

**Meta-analysis.** To exclude possible scanner and site effects, we repeated the ROI-based correlation analyses of UrbanSat with neuroimaging measures in each site (both CHIMGEN and IMAGEN) and performed meta-analysis to integrate the results. The meta-analyses pooled each centre's effect size of correlation coefficient between UrbanSat and neuroimaging measure of each ROI, using an inverse variance-weighted random-effects model as implemented in the R package 'metafor' (version v2.1-0)<sup>61</sup> (Supplementary Methods). The Fisher's z-transformed correlation coefficient, standard errors (SE), z values, P values, CIs and measure of heterogeneity ( $I^2$  statistics) were computed in the meta-analysis (Supplementary Methods).

**Correlation analyses of mean UrbanSat with behaviour.** For the behavioural analysis, partial correlation analysis was firstly applied to test the correlation of UrbanSat with each neuropsychological domain and mental health in CHIMGEN under Bonferroni-corrected  $P_c < 0.05$  after controlling for the same confounding covariates. Bonferroni correction for the two data types and 21 items (Table 1 and Supplementary Table 15) was applied in CHIMGEN. We therefore set a significance threshold of Bonferroni-corrected  $P_c < 0.05$  (equal to an uncorrected  $P < (0.05/2/21) = 0.001$ ) in CHIMGEN. All the significant results would be replicated in IMAGEN at Bonferroni-corrected  $P_c < 0.05$  (equal to an uncorrected  $P < (0.05/4) = 0.013$ ), where we only include four measures of behaviour (IRI, RSQ, DAWBA-GA and CIDI-AS).

**Identification of susceptibility periods using a distributed lag model.** To account for within-subject autocorrelation and consider the delayed effect of longitudinal UrbanSat, we used a DLM to investigate susceptibility periods of lifetime UrbanSat on brain and behaviours by creating an UrbanSat lag space<sup>62</sup> (1–30 years in CHIMGEN). The DLM is defined through a 'cross-basis' function, which allows the simultaneous estimation of a linear exposure–response association and nonlinear lag-response association across lags. Specifically, we fitted the DLM as the following formula:

$$Y_i = \beta_0 + \sum_{j=1}^n [\alpha_j \text{UrbanSat}_{ij}] + \beta_1 X_{1i} + \beta_2 X_{2i} + \dots + \beta_p X_{pi}$$

Here  $\text{UrbanSat}_{ij}$  is the out-of-sample predicted UrbanSat score in age  $j$  of lifetime year  $n$ ,  $X_{1i}$  to  $X_{pi}$  are the same confounding covariates adjusted before for participant  $i$ . To account for collinearity among the yearly UrbanSat, we fitted constrained DLMs that assume these effects  $\alpha_j$  are a smooth function of  $j$  year. Therefore, the DLM model simultaneously integrates the data from all time points and assumes that the association between the UrbanSat and brain/behaviour at a given time point, controlling for UrbanSat at all other time points, varies smoothly as a function of time. The smooth function of lag structure was modelled using a natural cubic spline with five degrees of freedom, setting the knots at equally spaced values on the lag scale (1–30 years). The number of knots was chosen based on the AIC. A susceptibility period is identified when the estimated pointwise 95% confidence intervals do not include zero.

**Multiple mediation analysis.** In the well-replicated UrbanSat–behaviour correlations in both datasets, multiple mediation analysis, an extension of mediation analysis<sup>63,64</sup>, was applied to formally test whether the UrbanSat–behaviour relationship can be mediated by brain structure and function while controlling confounding covariates and other mediators (Supplementary Methods).

**Reporting summary.** Further information on research design is available in the Nature Research Summary linked to this article.

## Data availability

All the data are available from the authors upon reasonable request and with permissions of the CHIMGEN and IMAGEN consortia.

## Code availability

Custom code that supports the findings of this study is available from the corresponding author upon request.

Received: 25 January 2021; Accepted: 26 August 2021;  
Published online: 28 October 2021

## References

- Prince, M. et al. No health without mental health. *Lancet* **370**, 859–877 (2007).
- van Os, J., Kenis, G. & Rutten, B. P. The environment and schizophrenia. *Nature* **468**, 203 (2010).
- Bick, J. & Nelson, C. A. Early adverse experiences and the developing brain. *Neuropsychopharmacology* **41**, 177 (2016).
- Bhugra, D., Ventriglio, A., Castaldelli-Maia, J., & McCay, L. *Urban Mental Health* (Oxford Univ. Press, 2019).
- Vlahov, D. & Galea, S. Urbanization, urbanicity, and health. *J. Urban Health* **79**, S1–S12 (2002).
- Heilig, G. K. *World Urbanization Prospects: The 2011 Revision* (United Nations DESA, 2012).
- 2018 Revision of World Urbanization Prospects* (United Nations, 2018).
- Evans, G. W. The built environment and mental health. *J. Urban Health* **80**, 536–555 (2003).
- Melchiorri, M. et al. Unveiling 25 years of planetary urbanization with remote sensing: perspectives from the global human settlement layer. *Remote Sens* **10**, 768 (2018).
- Selentrich, N. Remote-sensing applications for environmental health research. *Environ. Health Perspect.* **122**, A268–A275 (2014).
- Xu, Q. et al. CHIMGEN: a Chinese imaging genetics cohort to enhance cross-ethnic and cross-geographic brain research. *Mol. Psychiatry* **25**, 517–529 (2020).
- Schumann, G. et al. The IMAGEN study: reinforcement-related behaviour in normal brain function and psychopathology. *Mol. Psychiatry* **15**, 1128–1139 (2010).
- Yeo, B. T. et al. The organization of the human cerebral cortex estimated by intrinsic functional connectivity. *J. Neurophysiol.* **106**, 1125–1165 (2011).
- Greicius, M. D., Krasnow, B., Reiss, A. L. & Menon, V. Functional connectivity in the resting brain: a network analysis of the default mode hypothesis. *Proc. Natl. Acad. Sci. USA* **100**, 253–258 (2003).
- Seeley, W. W. et al. Dissociable intrinsic connectivity networks for salience processing and executive control. *J. Neurosci.* **27**, 2349–2356 (2007).
- Lamm, C., Batson, C. D. & Decety, J. The neural substrate of human empathy: effects of perspective-taking and cognitive appraisal. *J. Cogn. Neurosci.* **19**, 42–58 (2007).
- Peen, J., Schoevers, R. A., Beekman, A. T. & Dekker, J. The current status of urban–rural differences in psychiatric disorders. *Acta Psychiatr. Scand.* **121**, 84–93 (2010).
- Weiser, M. et al. Social and cognitive functioning, urbanicity and risk for schizophrenia. *Br. J. Psychiatry* **191**, 320–324 (2007).
- Hiser, J. & Koenigs, M. The multifaceted role of the ventromedial prefrontal cortex in emotion, decision making, social cognition, and psychopathology. *Biol. Psychiatry* **83**, 638–647 (2018).
- Henckens, M. J. et al. Stress-induced alterations in large-scale functional networks of the rodent brain. *Neuroimage* **105**, 312–322 (2015).
- Pujol, J. et al. Traffic pollution exposure is associated with altered brain connectivity in school children. *Neuroimage* **129**, 175–184 (2016).
- Haddad, L. et al. Brain structure correlates of urban upbringing, an environmental risk factor for schizophrenia. *Schizophr. Bull.* **41**, 115–122 (2015).
- Schmahmann, J. D. & Sherman, J. C. The cerebellar cognitive affective syndrome. *Brain* **121**, 561–579 (1998).
- Bambico, F. R. et al. High frequency stimulation of the anterior vermis modulates behavioural response to chronic stress: involvement of the prefrontal cortex and dorsal raphe? *Neurobiol. Dis.* **116**, 166–178 (2018).
- Carta, I., Chen, C. H., Schott, A. L., Dorizan, S. & Khodakhal, K. Cerebellar modulation of the reward circuitry and social behavior. *Science* **363**, 6424 (2019).
- Middleton, F. A. & Strick, P. L. Cerebellar projections to the prefrontal cortex of the primate. *J. Neurosci.* **21**, 700–712 (2001).
- Shaw, P. et al. Neurodevelopmental trajectories of the human cerebral cortex. *J. Neurosci.* **28**, 3586–3594 (2008).
- Lenroot, R. K. & Giedd, J. N. Brain development in children and adolescents: insights from anatomical magnetic resonance imaging. *Neurosci. Biobehav. Rev.* **30**, 718–729 (2006).
- Tiemeier, H. et al. Cerebellum development during childhood and adolescence: a longitudinal morphometric MRI study. *Neuroimage* **49**, 63–70 (2010).
- Lederbogen, F. et al. City living and urban upbringing affect neural social stress processing in humans. *Nature* **474**, 498–501 (2011).
- Price, C., Dalman, C., Zammit, S. & Kirkbride, J. B. Association of residential mobility over the life course with nonaffective psychosis in 1.4 million young people in Sweden. *JAMA Psychiatry* **75**, 1128–1136 (2018).
- Fuhrmann, D., Knoll, L. J. & Blakemore, S. J. Adolescence as a sensitive period of brain development. *Trends Cogn. Sci.* **19**, 558–566 (2015).
- Tang, Y. et al. Brain structure differences between Chinese and Caucasian cohorts: a comprehensive morphometry study. *Hum. Brain Mapp.* **39**, 2147–2155 (2018).

34. Bremner, J. D. Stress and brain atrophy. *CNS Neurol. Disord. Drug Targets* **5**, 503–512 (2006).
35. Guxens, M. et al. Air pollution exposure during fetal life, brain morphology, and cognitive function in school-age children. *Biol. Psychiatry* **84**, 295–303 (2018).
36. Khan, A. et al. Environmental pollution is associated with increased risk of psychiatric disorders in the US and Denmark. *PLoS Biol.* **17**, e3000353 (2019).
37. Tyborowska, A. et al. Early-life and pubertal stress differentially modulate grey matter development in human adolescents. *Sci. Rep.* **8**, 9201 (2018).
38. Paus, T. Mapping brain maturation and cognitive development during adolescence. *Trends Cogn. Sci.* **9**, 60–68 (2005).
39. Callaghan, B. L. & Tottenham, N. The stress acceleration hypothesis: effects of early-life adversity on emotion circuits and behavior. *Curr. Opin. Behav. Sci.* **7**, 76–81 (2016).
40. Fonken, L. K. et al. Air pollution impairs cognition, provokes depressive-like behaviors and alters hippocampal cytokine expression and morphology. *Mol. Psychiatry* **16**, 987–995 (2011).
41. Elvidge, C. D. et al. Radiance calibration of DMSP-OLS low-light imaging data of human settlements. *Remote Sens. Environ.* **68**, 77–88 (1999).
42. Liu, Z. et al. Extracting the dynamics of urban expansion in China using DMSP-OLS nighttime light data from 1992 to 2008. *Landscape. Urban Plan.* **106**, 62–72 (2012).
43. Ma, T., Zhou, C., Pei, T., Haynie, S. & Fan, J. J. R. S. O. E. Quantitative estimation of urbanization dynamics using time series of DMSP/OLS nighttime light data: a comparative case study from China's cities. *Remote Sens. Environ.* **124**, 99–107 (2012).
44. Ghosh, T. et al. Shedding light on the global distribution of economic activity. *Open Geogr. J.* **3**, 147–160 (2010).
45. Helbich, M. J. Spatiotemporal contextual uncertainties in green space exposure measures: exploring a time series of the normalized difference vegetation indices. *Int. J. Environ. Res. Public Health* **16**, 852 (2019).
46. Zhou, Y. et al. A global map of urban extent from nightlights. *Environ. Res. Lett.* **10**, 054011 (2015).
47. Esau, I. et al. Trends in normalized difference vegetation index (NDVI) associated with urban development in northern West Siberia. *Atmos. Chem. Phys.* **16**, 9563–9577 (2016).
48. Zha, Y., Gao, J. & Ni, S. J. Use of normalized difference built-up index in automatically mapping urban areas from TM imagery. *Int. J. Remote Sens.* **24**, 583–594 (2003).
49. McFeeters, S. K. The use of the normalized difference water index (NDWI) in the delineation of open water features. *Int. J. Remote Sens.* **17**, 1425–1432 (1996).
50. Foley, J. A. et al. Global consequences of land use. *Science* **309**, 570–574 (2005).
51. Gong, P. et al. Finer resolution observation and monitoring of global land cover: first mapping results with Landsat TM and ETM+ data. *Int. J. Remote Sens.* **34**, 2607–2654 (2013).
52. Liu, X. et al. Identifying patterns and hotspots of global land cover transitions using the ESA CCI Land Cover dataset. *Remote Sens. Lett.* **9**, 972–981 (2018).
53. Ashburner, J. & Ridgway, G. R. Symmetric diffeomorphic modeling of longitudinal structural MRI. *Front. Neurosci.* **6**, 197 (2013).
54. Buuren, S. V. & Groothuis-Oudshoorn, K. mice: multivariate imputation by chained equations in R. *J. Stat. Softw.* **45**, 1–67 (2010).
55. Rosseel, Y. lavaan: an R package for structural equation modeling. *J. Stat. Softw.* **48**, 1–36 (2012).
56. Hoyle, R. H. *Structural Equation Modeling: Concepts, Issues, and Applications* (Sage, 1995).
57. Raykov, T. Bias-corrected estimation of noncentrality parameters of covariance structure models. *Struct. Equ. Modeling* **12**, 120–129 (2005).
58. Brown, T. A. *Confirmatory Factor Analysis for Applied Research* (Guilford, 2014).
59. Rubin, D. B. *Multiple Imputation for Nonresponse in Surveys* (Wiley, 2004).
60. Mollink, J. et al. The spatial correspondence and genetic influence of interhemispheric connectivity with white matter microstructure. *Nat. Neurosci.* **22**, 809 (2019).
61. Viechtbauer, W. Conducting meta-analysis in R with the metafor package. *J. Stat. Softw.* **36**, 1–48 (2010).
62. Gasparrini, A. J. Distributed lag linear and non-linear models in R: the package dlnm. *J. Stat. Softw.* **43**, 1 (2011).
63. Preacher, K. J. & Hayes, A. F. Asymptotic and resampling strategies for assessing and comparing indirect effects in multiple mediator models. *Behav. Res Methods* **40**, 879–891 (2008).
64. Hayes, A. F. *Introduction to Mediation, Moderation, and Conditional Process Analysis: a Regression-Based Approach* (Guilford, 2013).

## Acknowledgements

This work was partly supported by the National Key Research and Development Program of China (grant no. 2018YFC1314301 to C.Y.), National Natural Science Foundation of China (grant no. 82001797 to J.X., 82030053 to C.Y., 81801687 to Q. Li and 81701668 to H.L.), National Key Research and Development Program of China (grant no. 2017YFA0604401 to L.Y. and 2019YFA0606601 to L.Y.), National Key Scientific and Technological Infrastructure project 'Earth System Science Numerical Simulator Facility' (EarthLab), European Union-funded FP6 Integrated Project IMAGEN (Reinforcement-related behaviour in normal brain function and psychopathology) (LSHM-CT-2007-037286), the Horizon 2020 funded ERC Advanced Grant 'STRATIFY' (Brain network based stratification of reinforcement-related disorders) (695313), ERANID (Understanding the Interplay between Cultural, Biological and Subjective Factors in Drug Use Pathways) (PR-ST-0416-10004), Human Brain Project (HBP SGA 2, 785907 and HBP SGA 3, 945539), Medical Research Council Grant 'c-VEDA' (Consortium on Vulnerability to Externalizing Disorders and Addictions) (MR/N000390/1), National Institute of Health (NIH) (R01DA049238, A decentralized macro and micro gene-by-environment interaction analysis of substance use behaviour and its brain biomarkers), National Institute for Health Research (NIH) Biomedical Research Centre at South London and Maudsley NHS Foundation Trust and King's College London, Bundesministerium für Bildung und Forschung (BMBF grants 01GS08152; 01EV0711; Forschungsnetz AERIAL 01EE1406A, 01EE1406B), Deutsche Forschungsgemeinschaft (DFG grants SM 80/7-2, SFB 940, TRR 265, NE 1383/14-1), Medical Research Foundation and Medical Research Council (grants MR/R00465X/1 and MR/S020306/1) and National Institutes of Health (NIH) funded ENIGMA (grants 5U54EB020403-05 and 1R56AG058854-01). Further support was provided by grants from the ANR (ANR-12-SAMA-0004, AAPG2019-GeBra), Eranet Neuron (AF12-NEUR0008-01-WM2NA; and ANR-18-NEUR0002-01- ADORé), Fondation de France (00081242), Fondation pour la Recherche Médicale (DPA20140629802), Mission Interministérielle de Lutte contre les Drogues et les Conduttes Addictives (MILDECA), Assistance-Publique-Hôpitaux-de-Paris and INSERM (interface grant), Paris Sud University IDEX 2012, Fondation de l'Avenir (grant AP-RM-17-013), Fédération pour la Recherche sur le Cerveau; National Institutes of Health, Science Foundation Ireland (16/ERC/3797), U.S.A. (Axon, Testosterone and Mental Health during Adolescence; RO1 MH085772-01A1), and NIH Consortium grant U54 EB020403, supported by a cross-NIH alliance that funds Big Data to Knowledge Centres of Excellence and The Science&Technology Development Fund of Tianjin Education Commission for Higher Education (grant no. 2019KJ195 to J.X.). Funded by the Deutsche Forschungsgemeinschaft (DFG, German Research Foundation) under Germany's Excellence Strategy – EXC-2049 – 390688087 Falls mehrere Projekte genannt werden müssen, könnte man das z.B. so gestalten: This work was supported by the Deutsche Forschungsgemeinschaft (Collaborative Research Grant SFB 958 (to DS (A5), SJS (A3, A6), CR (A5)) and Excellence Strategy – EXC-2049–390688087 (to DS, SJS, and CR)). The authors thank C. Li, Department of Health Statistics, College of Public Health, Tianjin Medical University for statistical advice. The funders had no role in study design, data collection and analysis, decision to publish or preparation of the manuscript.

## Author contributions

G.S., C.Y. and J.X. designed the study. J.X., C.Y. and G.S. wrote the manuscript. All authors critically reviewed the manuscript. X.L., Q. Li, R.G., W.Q., F.L., C.C., Q. Luo, A.I., L.G., N.L., H.L., C.H., K.P., V.C., M.J.L., M.L., P.G., E.D.B., N.C., A.M., L.Y., C.Y. and G.S. were the principal investigators. J.C., M.W., Z.G., W.Z., B.Z., W.L., S.Q., H.Z., X.X., Y.Y., B.G., T.H., G.C., F.C., J.X., J.L., J.Z., X.Z., D.W., W.S., Y.M., F.Y., S.L., X.Z., K.X., L.Z., Z.Y., T.B., G.B., A.L.W.B., H.F., A.G., H.G., P.G., A.H., R.B., J.M., E.A., F.N., D.P.O., H. L., T.P., L.P., L.R., S.H., J.H.E., M.N.S., H.W., R.W. and J.W. acquired the data. A.M. supervised the statistical analysis. J.X. and Q. Li analysed the data.

## Competing interests

The authors declare no competing interests.

## Additional information

**Extended data** is available for this paper at <https://doi.org/10.1038/s41562-021-01204-7>.

**Supplementary information** The online version contains supplementary material available at <https://doi.org/10.1038/s41562-021-01204-7>.

**Correspondence and requests for materials** should be addressed to Chunshui Yu or Gunter Schumann.

**Peer review information** *Nature Human Behaviour* thanks the anonymous reviewers for their contribution to the peer review of this work. Peer reviewer reports are available.

**Reprints and permissions information** is available at [www.nature.com/reprints](http://www.nature.com/reprints).

**Publisher's note** Springer Nature remains neutral with regard to jurisdictional claims in published maps and institutional affiliations.

© The Author(s), under exclusive licence to Springer Nature Limited 2021

<sup>1</sup>Department of Radiology and Tianjin Key Laboratory of Functional Imaging, Tianjin Medical University General Hospital, Tianjin, P. R. China. <sup>2</sup>Centre for Population Neuroscience and Precision Medicine (PONS), Institute of Psychiatry, Psychology and Neuroscience, SGDP Centre, King's College London, London, UK. <sup>3</sup>Ministry of Education Key Laboratory for Earth System Modeling, Department of Earth System Science, Tsinghua University, Beijing, P. R. China. <sup>4</sup>College of Information Engineering, Tianjin University of Commerce, Tianjin, P. R. China. <sup>5</sup>New Light Technologies Inc., Washington, DC, USA. <sup>6</sup>Institute of Science and Technology for Brain-Inspired Intelligence, Ministry of Education-Key Laboratory of Computational Neuroscience and Brain-Inspired Intelligence, Fudan University, Shanghai, China. <sup>7</sup>State Key Laboratory of Medical Neurobiology and MOE Frontiers Center for Brain Science, Institutes of Brain Science and Human Phenome Institute, Fudan University, Shanghai, China. <sup>8</sup>Department of Magnetic Resonance Imaging, First Affiliated Hospital of Zhengzhou University, Zhengzhou, China. <sup>9</sup>Department of Radiology, Zhengzhou University People's Hospital and Henan Provincial People's Hospital, Zhengzhou, China. <sup>10</sup>Department of Medical Imaging, Second Hospital of Hebei Medical University, Shijiazhuang, China. <sup>11</sup>Department of Radiology, Tongji Hospital, Tongji Medical College, Huazhong University of Science and Technology, Wuhan, China. <sup>12</sup>Department of Radiology, Drum Tower Hospital, Medical School of Nanjing University, Nanjing, China. <sup>13</sup>Department of Radiology, Xiangya Hospital, Central South University, Changsha, China. <sup>14</sup>Department of Medical Imaging, First Affiliated Hospital of Guangzhou University of Chinese Medicine, Guangzhou, China. <sup>15</sup>Department of Radiology, The First Hospital of Shanxi Medical University, Taiyuan, China. <sup>16</sup>Department of Radiology, Second Affiliated Hospital of Zhejiang University, School of Medicine, Hangzhou, China. <sup>17</sup>Department of Radiology, First Affiliated Hospital of Anhui Medical University, Hefei, China. <sup>18</sup>Department of Radiology, Affiliated Hospital of Guizhou Medical University, Guiyang, Guizhou, China. <sup>19</sup>Department of Radiology, Tianjin Huanhu Hospital, Tianjin, China. <sup>20</sup>Functional and Molecular Imaging Key Lab of Shaanxi Province and Department of Radiology, Tangdu Hospital, Military Medical University of PLA Airforce (Fourth Military Medical University), Xi'an, China. <sup>21</sup>Department of Radiology, Hainan General Hospital, Haikou, China. <sup>22</sup>Department of Radiology, Beijing Tongren Hospital, Capital Medical University, Beijing, China. <sup>23</sup>Department of Radiology, First Affiliated Hospital of Wenzhou Medical University, Wenzhou, China. <sup>24</sup>Department of Magnetic Resonance, Lanzhou University Second Hospital, Lanzhou, China. <sup>25</sup>State Key Laboratory of Cognitive Neuroscience and IDG/McGovern Institute for Brain Research, Beijing Normal University, Beijing, China. <sup>26</sup>Department of Radiology, Qilu Hospital of Shandong University, Jinan, China. <sup>27</sup>Department of Radiology, Tianjin First Center Hospital, Tianjin, China. <sup>28</sup>Department of Radiology, First Affiliated Hospital of Dalian Medical University, Dalian, China. <sup>29</sup>Department of Radiology, Pingjin Hospital, Logistics University of Chinese People's Armed Police Forces, Tianjin, China. <sup>30</sup>Department of Radiology, Center for Medical Imaging, West China Hospital of Sichuan University, Chengdu, China. <sup>31</sup>Department of Radiology, First Affiliated Hospital of USTC, Hefei National Laboratory for Physical Sciences at the Microscale and School of Life Science, Division of Life Science and Medicine, University of Science and Technology of China, Hefei, China. <sup>32</sup>Department of Radiology, Affiliated Hospital of Xuzhou Medical University, Xuzhou, China. <sup>33</sup>Department of Medical Imaging, Jinling Hospital, Medical School of Nanjing University, Nanjing, China. <sup>34</sup>Department of Radiology, Tianjin Medical University Cancer Institute and Hospital, Tianjin, China. <sup>35</sup>Department of Child and Adolescent Psychiatry and Psychotherapy, Central Institute of Mental Health, Medical Faculty Mannheim, Heidelberg University, Mannheim, Germany. <sup>36</sup>Department of Neuroimaging, Institute of Psychiatry, Psychology & Neuroscience, King's College London, London, UK. <sup>37</sup>Discipline of Psychiatry, School of Medicine and Trinity College Institute of Neuroscience, Trinity College Dublin, Dublin, Ireland. <sup>38</sup>Department of Cognitive and Clinical Neuroscience, Central Institute of Mental Health, Medical Faculty Mannheim, Heidelberg University, Mannheim, Germany. <sup>39</sup>Department of Psychology, School of Social Sciences, University of Mannheim, Mannheim, Germany. <sup>40</sup>NeuroSpin, CEA, Université Paris-Saclay, Gif-sur-Yvette, France. <sup>41</sup>Department of Psychiatry and Psychology, University of Vermont, Burlington, VT, USA. <sup>42</sup>Sir Peter Mansfield Imaging Centre School of Physics and Astronomy, University of Nottingham, Nottingham, UK. <sup>43</sup>Charité - Universitätsmedizin Berlin, Corporate Member of Freie Universität Berlin, Humboldt-Universität zu Berlin, and Berlin Institute of Health, Department of Psychiatry and Psychotherapy, Berlin, Germany. <sup>44</sup>Physikalisch-Technische Bundesanstalt (PTB), Berlin, Germany. <sup>45</sup>Ecole Normale Supérieure Paris-Saclay, Université Paris-Saclay, CNRS, Centre Borelli, INSERM U1299 "Trajectoires Développementales & Psychiatrie", Gif-sur-Yvette, France. <sup>46</sup>Institut National de la Santé et de la Recherche Médicale, INSERM Unit 1000 Neuroimaging and Psychiatry, University Paris Sud, University Paris Descartes - Sorbonne Paris Cité; Psychiatry Department 91G16, Orsay Hospital, Orsay, France. <sup>47</sup>Institute National de la Santé et de la Recherche Médicale, UMR 992 INSERM, CEA, Faculté de médecine, Université Paris-Sud, Université Paris-Saclay NeuroSpin, Gif-sur-Yvette, France. <sup>48</sup>Departments of Psychiatry and Neuroscience, Faculty of Medicine and Centre Hospitalier Universitaire Sainte-Justine, University of Montreal, Montreal, Quebec, Canada. <sup>49</sup>Departments of Psychology and Psychiatry, University of Toronto, Toronto, Ontario, Canada. <sup>50</sup>Department of Child and Adolescent Psychiatry and Psychotherapy, University Medical Centre Göttingen, Göttingen, Germany. <sup>51</sup>Department of Psychology, Institute of Psychiatry, Psychology and Neuroscience, King's College London, London, UK. <sup>52</sup>Department of Psychiatry and Neuroimaging Center, Technische Universität Dresden, Dresden, Germany. <sup>53</sup>School of Psychology and Global Brain Health Institute, Trinity College Dublin, Dublin, Ireland. <sup>54</sup>Department of Psychiatry and Psychotherapy CCM, Charité - Universitätsmedizin Berlin, Corporate Member of Freie Universität Berlin, Humboldt-Universität zu Berlin, and Berlin Institute of Health, Berlin, Germany. <sup>55</sup>Department of Education and Psychology, Freie Universität Berlin, Berlin, Germany. <sup>56</sup>Center for Wireless and Population Health Systems, Department of Family and Preventive Medicine and Calit2's Qualcomm Institute, University of California San Diego, La Jolla, CA, USA. <sup>57</sup>Tri-institutional Center for Translational Research in Neuroimaging and Data Science (TReNDS), Georgia State University, Georgia Institute of Technology, Emory University, Atlanta, GA, USA. <sup>58</sup>Collaborative Innovation Center of Tianjin for Medical Epigenetics, Tianjin Key Laboratory of Medical Epigenetics, Department of Pharmacology, Tianjin Medical University, Tianjin, P. R. China. <sup>59</sup>School of Medical Imaging and Tianjin Key Laboratory of Functional Imaging, Tianjin Medical University, Tianjin, P. R. China. <sup>60</sup>Department of Geography and Department of Earth Sciences, University of Hong Kong, Hong Kong, China. <sup>61</sup>Google, Inc., Mountain View, CA, USA. <sup>62</sup>Predictive Clinical Neuroscience Group at the Donders Institute, Radboud University Medical Center, Nijmegen, the Netherlands. <sup>63</sup>CAS Center for Excellence in Brain Science and Intelligence Technology, Chinese Academy of Sciences, Shanghai, P. R. China. <sup>64</sup>Centre for Population Neuroscience and Stratified Medicine (PONS), Institute for Science and Technology of Brain-Inspired Intelligence (ISTBI), Fudan University, Shanghai, P. R. China. <sup>65</sup>Centre for Population Neuroscience and Stratified Medicine (PONS), Charite Mental Health, Dept. of Psychiatry and Psychotherapy, CCM, Charite Universitätsmedizin Berlin, Berlin, Germany.

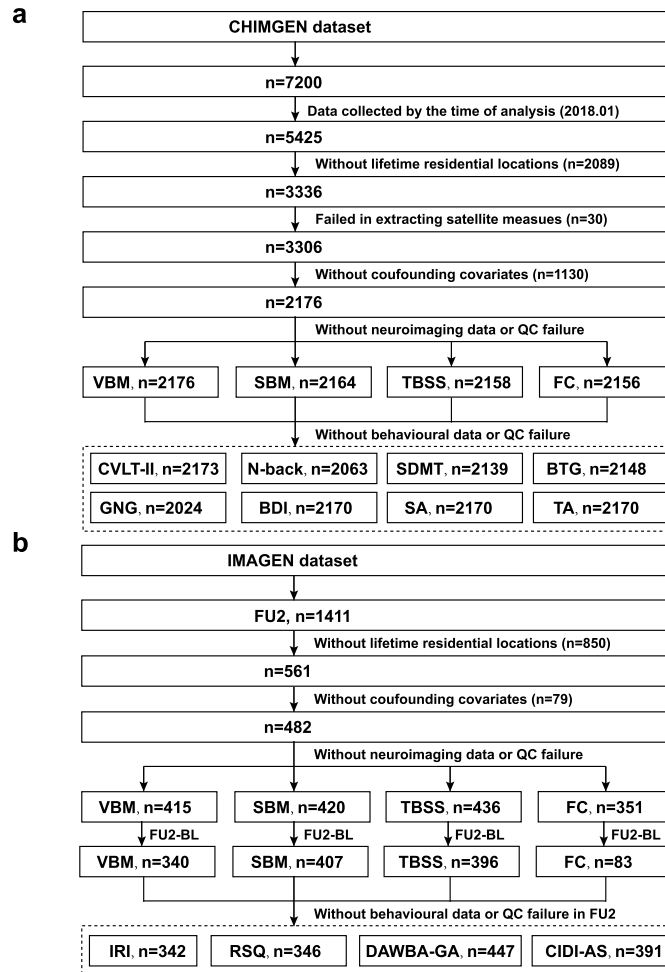
\*A list of authors and their affiliations appears at the end of the paper. ☰ e-mail: [chunshuiyu@tmu.edu.cn](mailto:chunshuiyu@tmu.edu.cn); [gunter.schumann1961@gmail.com](mailto:gunter.schumann1961@gmail.com)

## the CHIMGEN

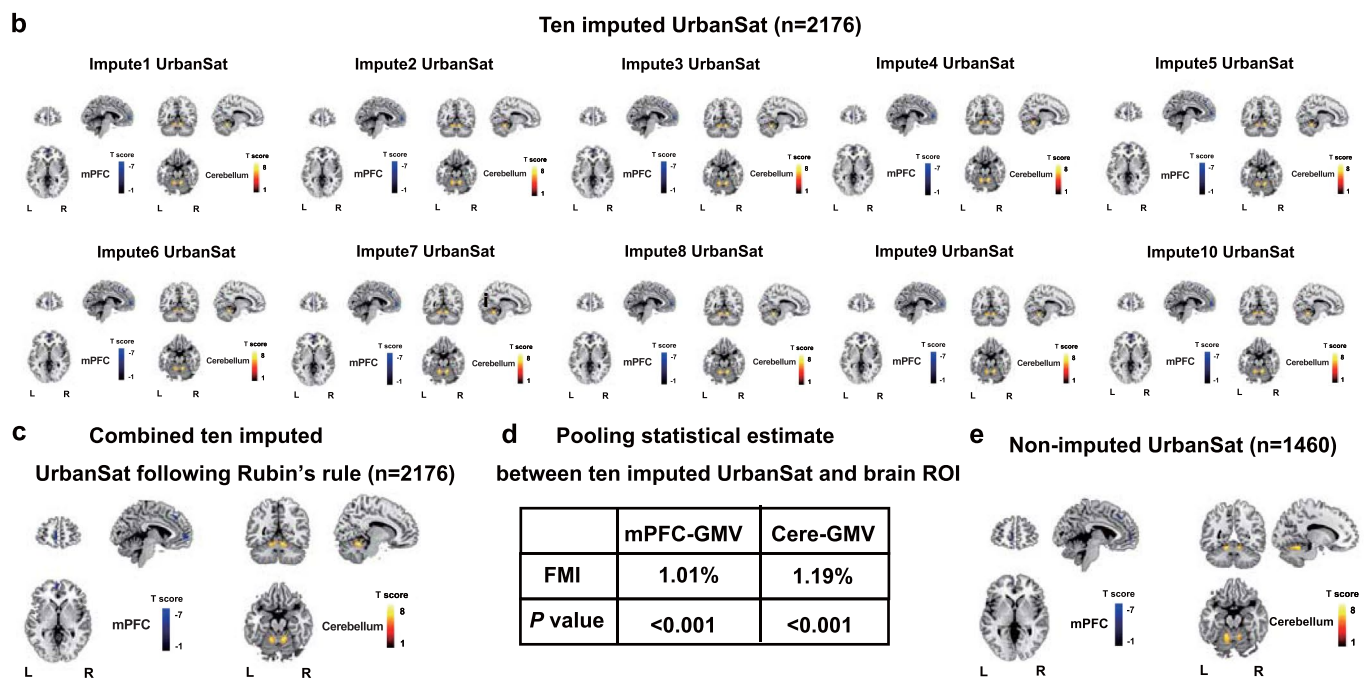
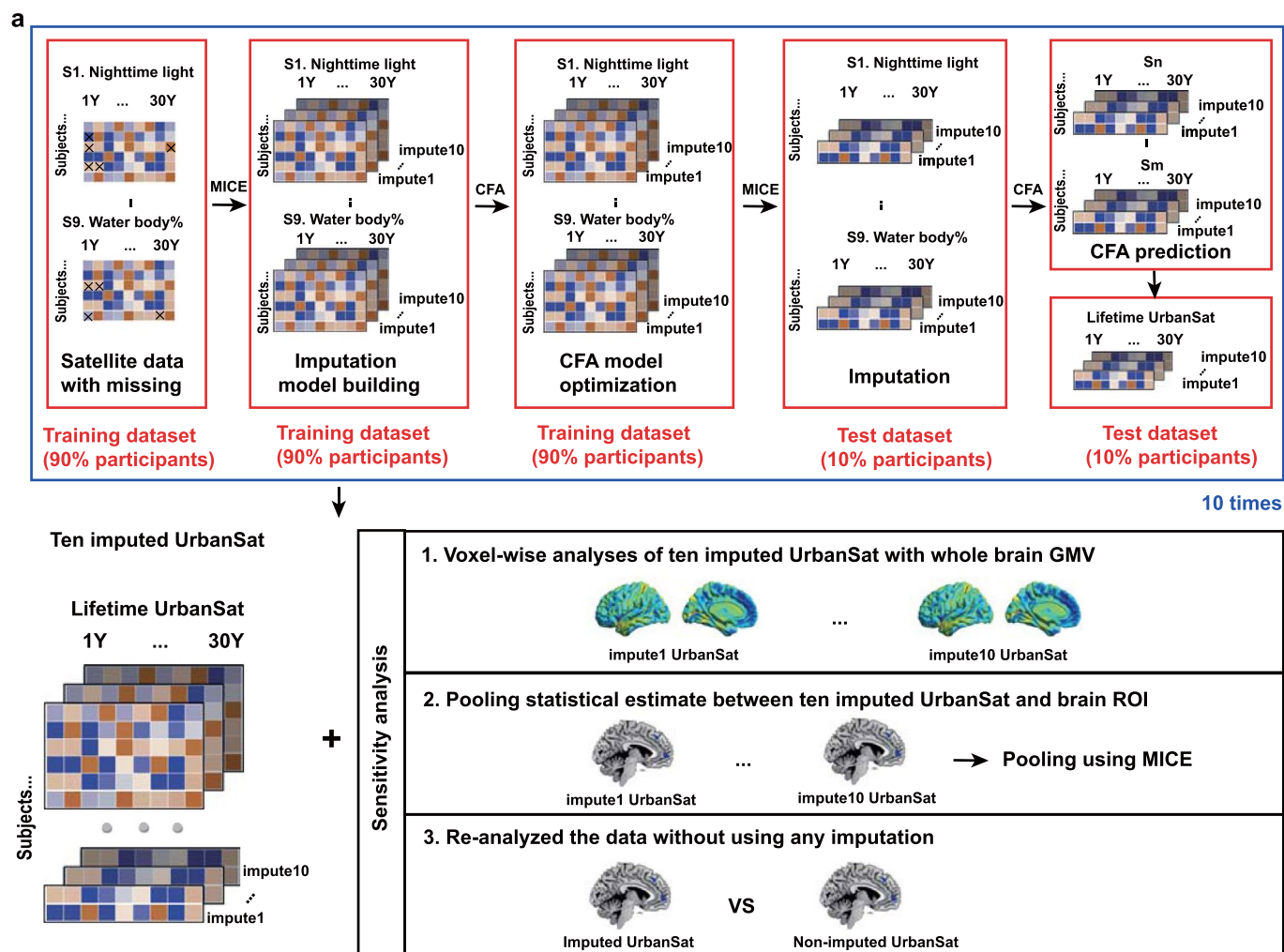
Jiayuan Xu<sup>1,2</sup>, Wen Qin<sup>1</sup>, Feng Liu<sup>1</sup>, Lining Guo<sup>1</sup>, Nana Liu<sup>1</sup>, Huaiwei Liu<sup>1</sup>, Jingliang Cheng<sup>8</sup>, Meiyun Wang<sup>9</sup>,  
 Zuojun Geng<sup>10</sup>, Wenzhen Zhu<sup>11</sup>, Bing Zhang<sup>12</sup>, Weihua Liao<sup>13</sup>, Shijun Qiu<sup>14</sup>, Hui Zhang<sup>15</sup>, Xiaojun Xu<sup>16</sup>,  
 Yongqiang Yu<sup>17</sup>, Bo Gao<sup>18</sup>, Tong Han<sup>19</sup>, Guangbin Cui<sup>20</sup>, Feng Chen<sup>21</sup>, Junfang Xian<sup>22</sup>, Jiance Li<sup>23</sup>,  
 Jing Zhang<sup>24</sup>, Xi-Nian Zuo<sup>25</sup>, Dawei Wang<sup>26</sup>, Wen Shen<sup>27</sup>, Yanwei Miao<sup>28</sup>, Fei Yuan<sup>29</sup>, Su Lui<sup>30</sup>,  
 Xiaochu Zhang<sup>31</sup>, Kai Xu<sup>32</sup>, Longjiang Zhang<sup>33</sup>, Zhaoxiang Ye<sup>34</sup>, Meng Liang<sup>59</sup> and Chunshui Yu<sup>1,63</sup>

**IMAGEN Consortia**

Tobias Banaschewski<sup>35</sup>, Gareth J. Barker<sup>36</sup>, Arun L. W. Bokde<sup>37</sup>, Herta Flor<sup>38,39</sup>, Antoine Grigis<sup>40</sup>, Hugh Garavan<sup>41</sup>, Penny Gowland<sup>42</sup>, Andreas Heinz<sup>43</sup>, Rüdiger Brühl<sup>44</sup>, Jean-Luc Martinot<sup>45</sup>, Eric Artiges<sup>46</sup>, Frauke Nees<sup>35,38</sup>, Dimitri Papadopoulos Orfanos<sup>40</sup>, Herve Lemaitre<sup>47</sup>, Tomáš Paus<sup>48,49</sup>, Luise Poustka<sup>50</sup>, Lauren Robinson<sup>51</sup>, Sarah Hohmann<sup>35</sup>, Julianne H. Fröhner<sup>52</sup>, Michael N. Smolka<sup>52</sup>, Henrik Walter<sup>43</sup>, Robert Whelan<sup>53</sup>, Jeanne Winterer<sup>54,55</sup>, Edward D. Barker<sup>51</sup> and Gunter Schumann<sup>64,65</sup>

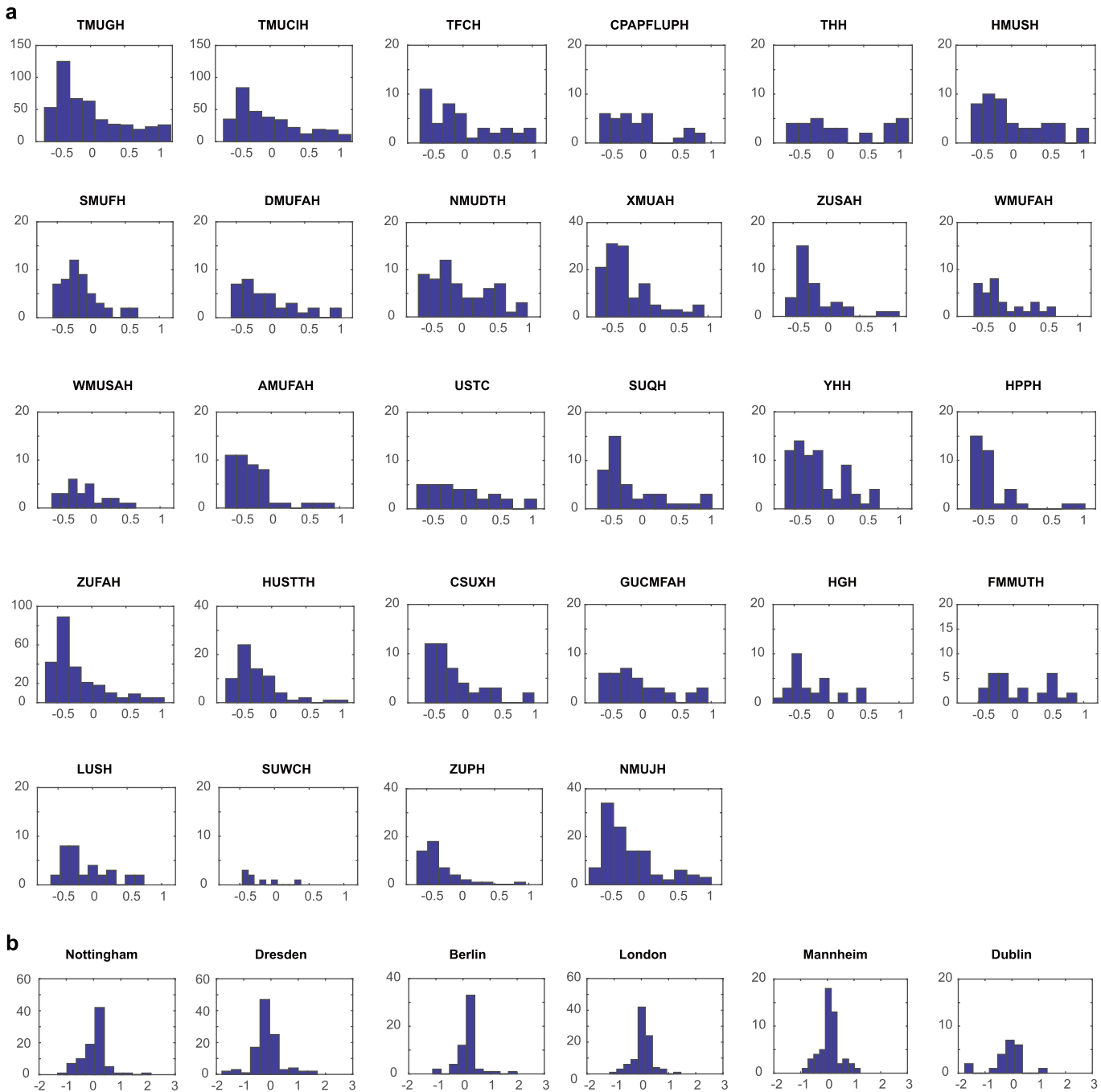


**Extended Data Fig. 1 | A flow diagram of sample selection in CHIMGEN (a) and IMAGEN (b).** BDI, Beck depression inventory; BTG, ball tossing games task; BL, IMAGEN baseline assessment acquired at 14 years; CIDI-AS, Anxiety Screening from the Composite International Diagnostic Interview; CVLT-II, the second edition of California verbal learning test; DAWBA-GA, Generalized Anxiety Scale from The Development and Well-Being Assessment Interview; FC, functional connectivity; FU2, IMAGEN second follow up assessment acquired at 19 years; FU2-BL, IMAGEN FU2-BL measures brain changes rate between BL of 14 years and FU2 of 19 years; GNG, go/no-go task; IRI, Interpersonal Reactivity Index; RSQ, Rumination Scale Questionnaire; SA, state anxiety; SBM, surface-based morphometry; SDMT, symbol digit modalities test; TA, trait anxiety; TBSS, tract-based spatial statistics; VBM, voxel-based morphometry.

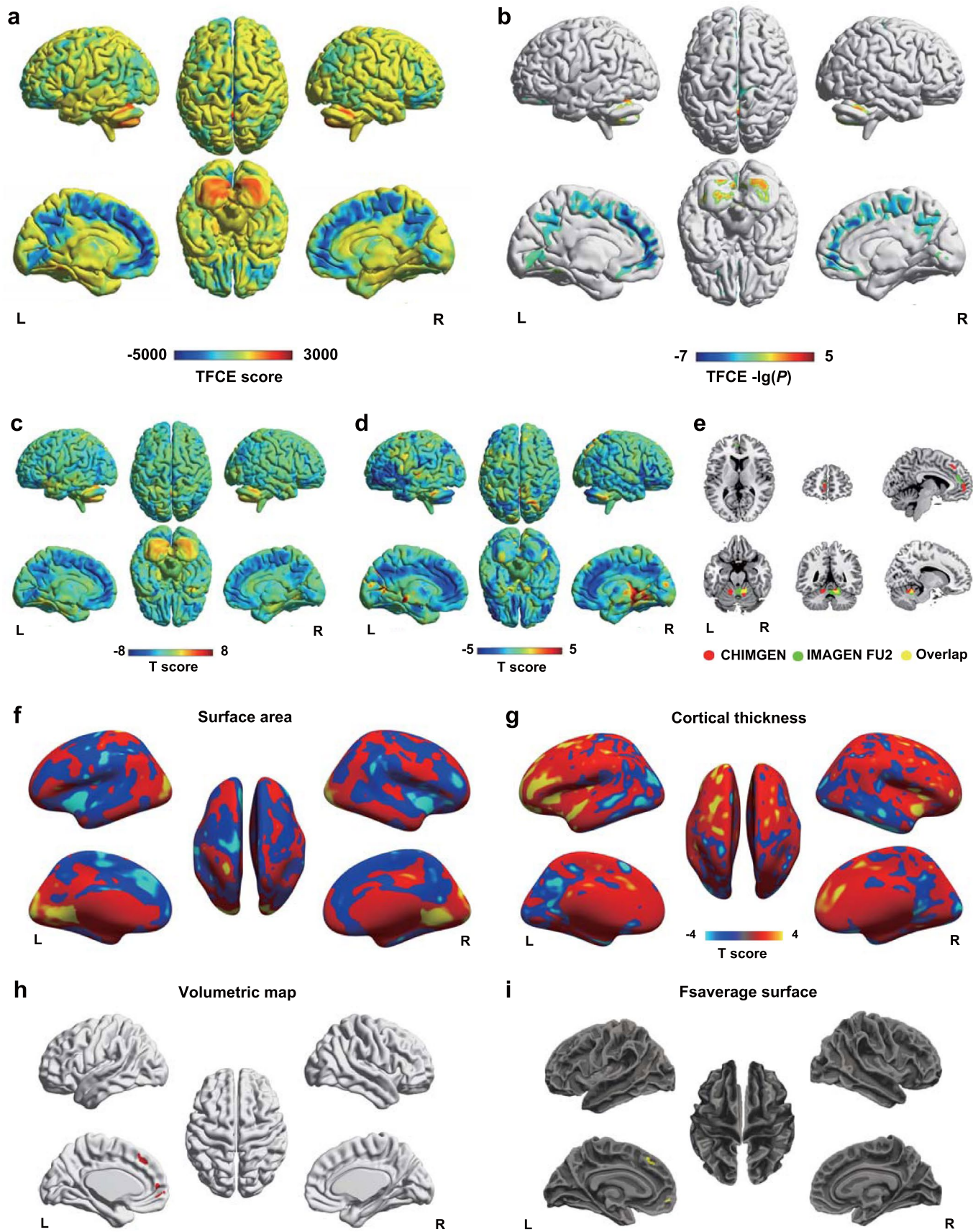


Extended Data Fig. 2 | See next page for caption.

**Extended Data Fig. 2 | Schematic summary of multiple imputation and confirmatory factor analysis.** **a.** A flow diagram for multiple imputation and confirmatory factor analysis. **b, c.** Sensitivity analysis results in voxel-wise correlations of ten imputed UrbanSat (**b**) and combined UrbanSat (**c**) with brain GMV in CHIMGEN (FWE  $P_c < 0.05$ ). Each imputed UrbanSat from MICE imputation before 18 years show a significant negative correlation with left mPFC volume and a significant positive correlation with cerebellar volume adjusting confounding covariates (FWE  $P_c < 0.05$ ) (**b**), similar to the results derived from combined UrbanSat score following Rubin's rule (**c**). **d.** The estimated fractions of missing information (FMI) of UrbanSat were low for the GMVs of left-mPFC-ROI (FMI = 1.01%) and cerebellum-ROI (FMI = 1.19%). UrbanSat was still correlated with mPFC-GMV ( $P < 0.001$ ) and cerebellum-GMV ( $P < 0.001$ ) after pooling using mice R package in CHIMGEN. **e.** Non-imputed mean UrbanSat before 18 years still show a significant negative correlation with mPFC-GMV and a significant positive correlation with cerebellar-GMV adjusting confounding covariates (FWE  $P_c < 0.05$ ) ( $n = 1460$ ). CFA, confirmatory factor analysis; FMI, fractions of missing information; L, left; MICE, multivariate imputation by chained equations; mPFC, medial prefrontal cortex; R, right. S, satellite; Y, years.

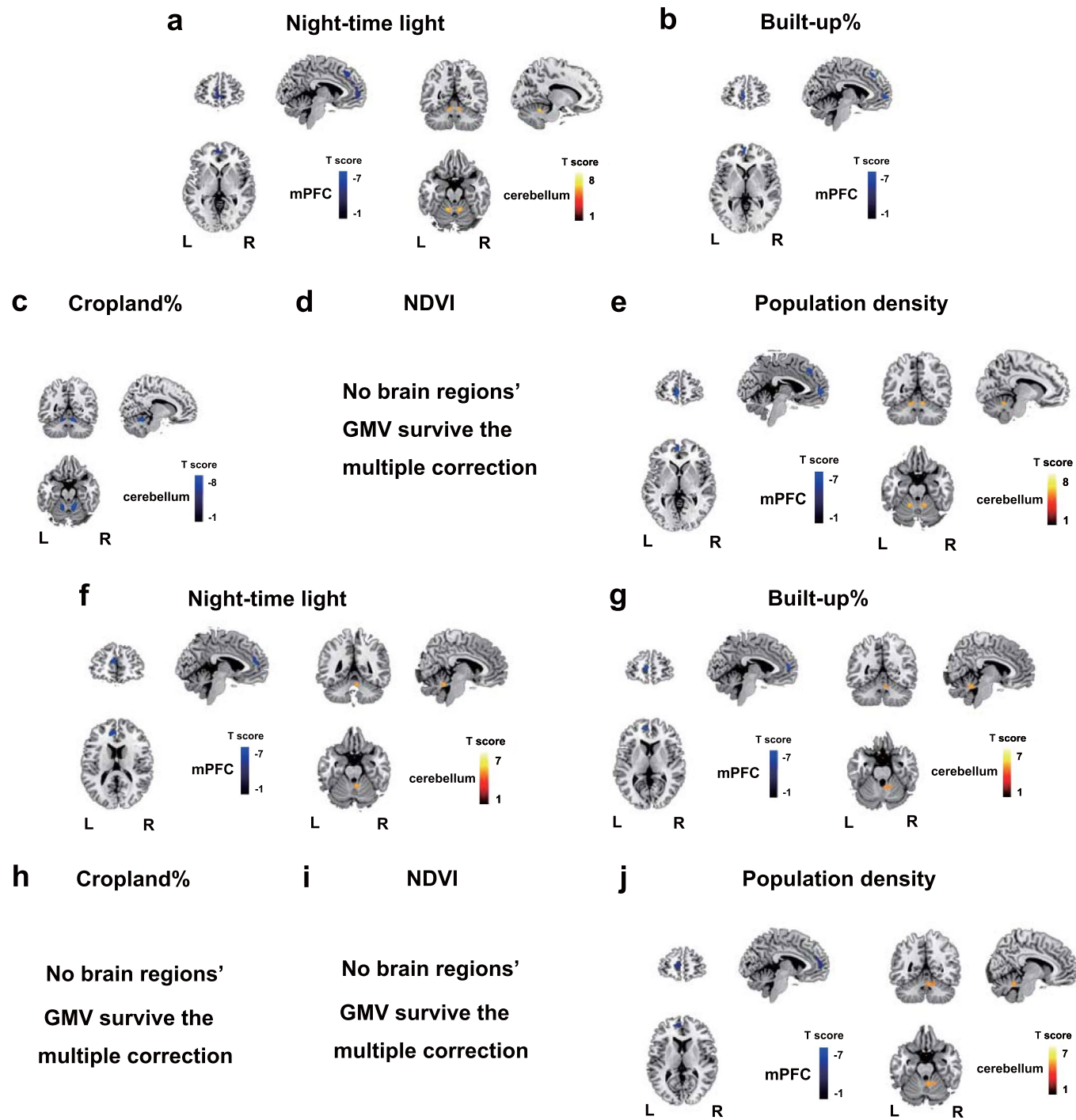


**Extended Data Fig. 3 | Histograms of UrbanSat in each center of CHIMGEN (a) and IMAGEN (b).** TMUGH, Tianjin Medical University General Hospital; TMUCIH, Tianjin Medical University Cancer Institute and Hospital; TFCH, Tianjin First Center Hospital; CPAPFLUPH, Pingjin Hospital, Logistics University of Chinese People's Armed Police Forces; THH, Tianjin Huanhu Hospital; HMUSH, The Second Hospital of Hebei Medical University; SMUFH, The First Hospital of Shanxi Medical University; DMUFAH, The First Affiliated Hospital of Dalian Medical University; NMUDTH, Drum Tower Hospital, Medical School of Nanjing University; XMUAH, The Affiliated Hospital of Xuzhou Medical University; ZUSAH, The Second Affiliated Hospital of Zhejiang University; VMUFAH, The First Affiliated Hospital of Wenzhou Medical University; WMUSAH, The Second Affiliated Hospital of Wenzhou Medical University; AMUFAH, The First Affiliated Hospital of Anhui Medical University; USTC, University of Science and Technology of China; SUQH, Qilu Hospital of Shandong University; YYH, Yantai Yuhuangding Hospital; ZUPH/HPPH, Zhengzhou University People's Hospital and Henan Provincial People's Hospital; ZUFAH, The First Affiliated Hospital of Zhengzhou University; HUSTTH, Tongji Hospital, Tongji Medical College, Huazhong University of Science and Technology; CSUXH, Xiangya Hospital, Central South University; GUCMFAH, The First Affiliated Hospital of Guangzhou University of Chinese Medicine; HGH, Hainan General Hospital; FMMUTH, Tangdu Hospital, the Military Medical University of PLA Airforce (Fourth Military Medical University); LUSH, Lanzhou University Second Hospital; SUWCH, West China Hospital of Sichuan University; ZUPH, Zhengzhou University People's Hospital; NMUJH, Jinling Hospital, Medical School of Nanjing University.

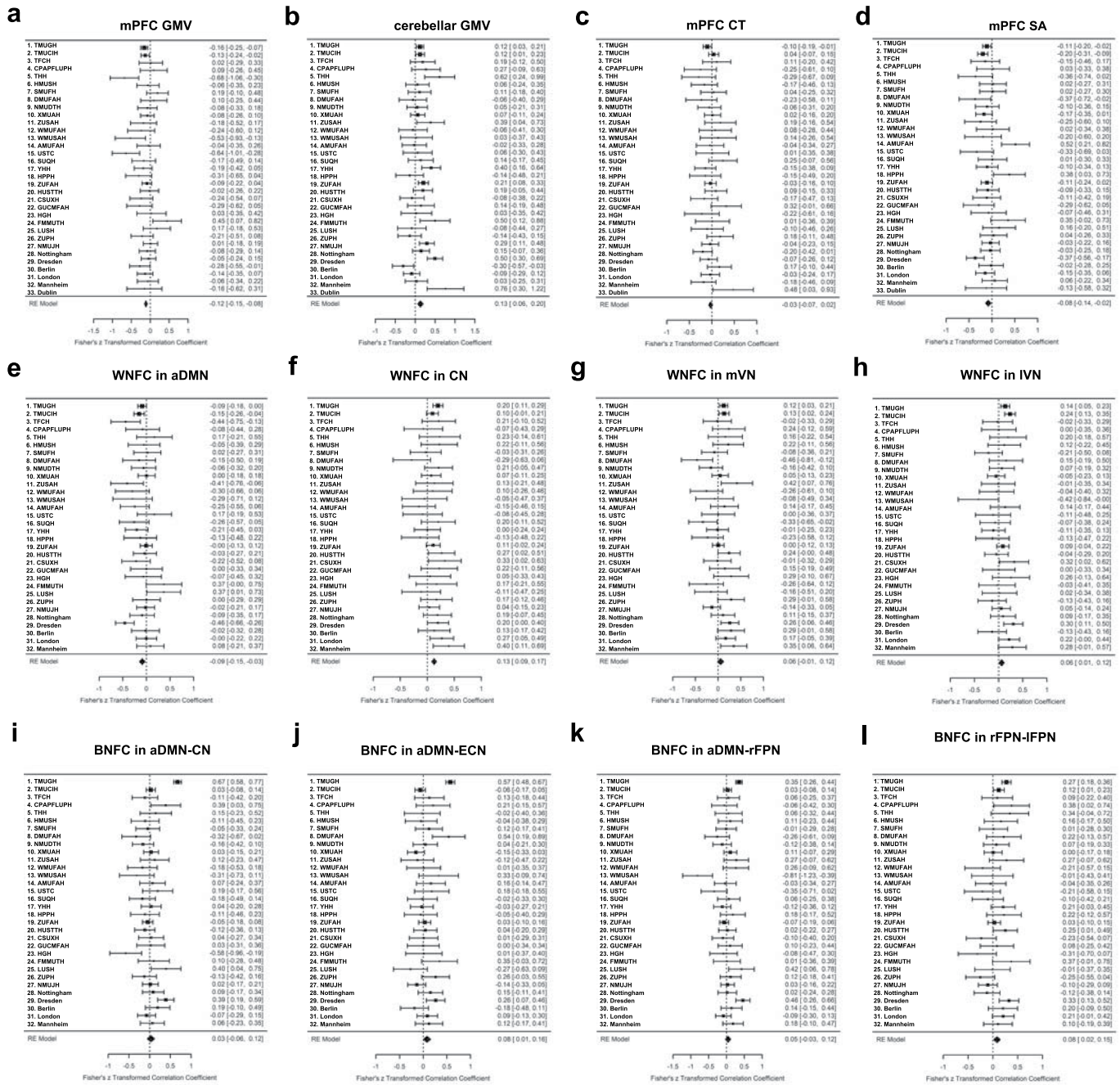


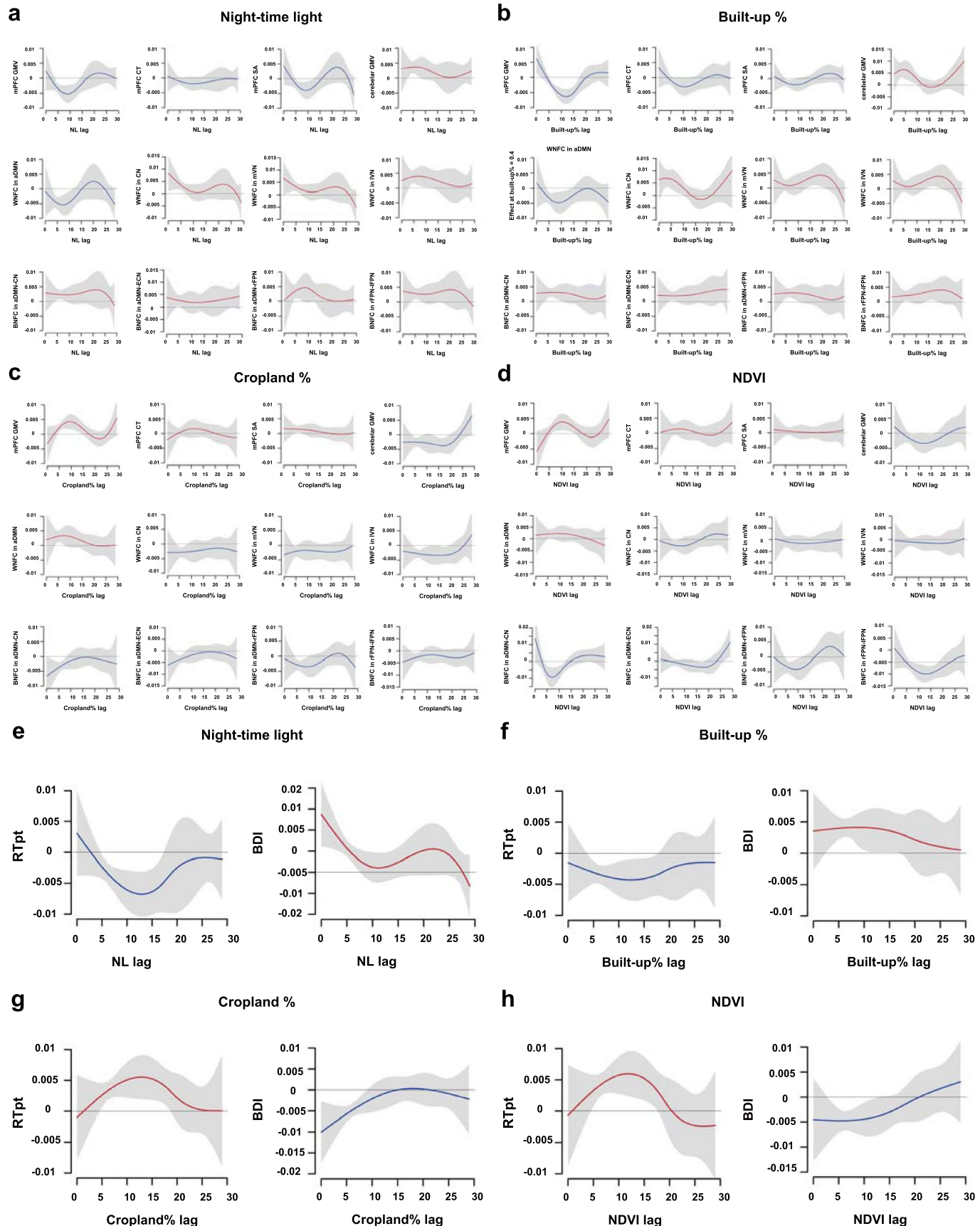
Extended Data Fig. 4 | See next page for caption.

**Extended Data Fig. 4 | Correlations of UrbanSat with brain GMV, SA and CT in CHIMGEN and IMAGEN.** **a.** Uncorrected correlation statistical maps of UrbanSat with brain GMV in CHIMGEN under non-parametric permutation testing ( $n=2176$ ). **b.** Correlations of UrbanSat with brain GMV in CHIMGEN under  $P_c < 0.05$  in TFCE-FWE using non-parametric permutation testing ( $n=2176$ ). **c, d.** Uncorrected correlation statistical maps of UrbanSat with brain GMV in CHIMGEN (**c**) and IMAGEN-FU2 (**d**) under parametric testing. **e.** The overlap results (yellow) in the voxel-wise correlation of mean UrbanSat before 18 years with brain GMV in CHIMGEN (red) and IMAGEN-FU2 (green) after controlling confounders (FWE  $P_c < 0.05$ ). **f, g.** Uncorrected vertex-wise correlation maps of UrbanSat with surface area (**f**) and cortical thickness (**g**) in CHIMGEN ( $n=2164$ ). **h, i.** The mPFC-ROI projected onto the volumetric map (**h**) and fsaverage surface in Freesurfer (**i**).



**Extended Data Fig. 5 | Voxel-wise correlations of individual satellite measures with brain GMV in CHIMGEN ( $n = 2176$ ) (a-e) and IMAGEN ( $n = 415$ ) (f-j).** **a-e.** In CHIMGEN, there are significant negative correlations of mean night-time light (a) and population density (e) with mPFC GMV and positive correlations with cerebellar GMV after controlling confounders (FWE,  $P_c < 0.05$ ); There are significant negative correlations of mean built-up with mPFC GMV (b) and of mean cropland with cerebellar GMV (c); There are no correlations of mean NDVI with brain GMV (d). **f-j.** In IMAGEN, there are significant negative correlations of mean night-time light (f), mean built-up (g) and population density (j) with mPFC GMV and positive correlations with cerebellar GMV after controlling confounders (FWE,  $P_c < 0.05$ ); There are no correlations of mean cropland (h) and NDVI (i) with brain GMV. L, left; mPFC, medial prefrontal cortex; NDVI, normalized difference vegetation index; R, right.





Extended Data Fig. 7 | See next page for caption.

**Extended Data Fig. 7 | Susceptibility analysis of individual satellite measures with brain (a-d) and behaviors (e-h) using distributed lag models in CHIMGEN.**

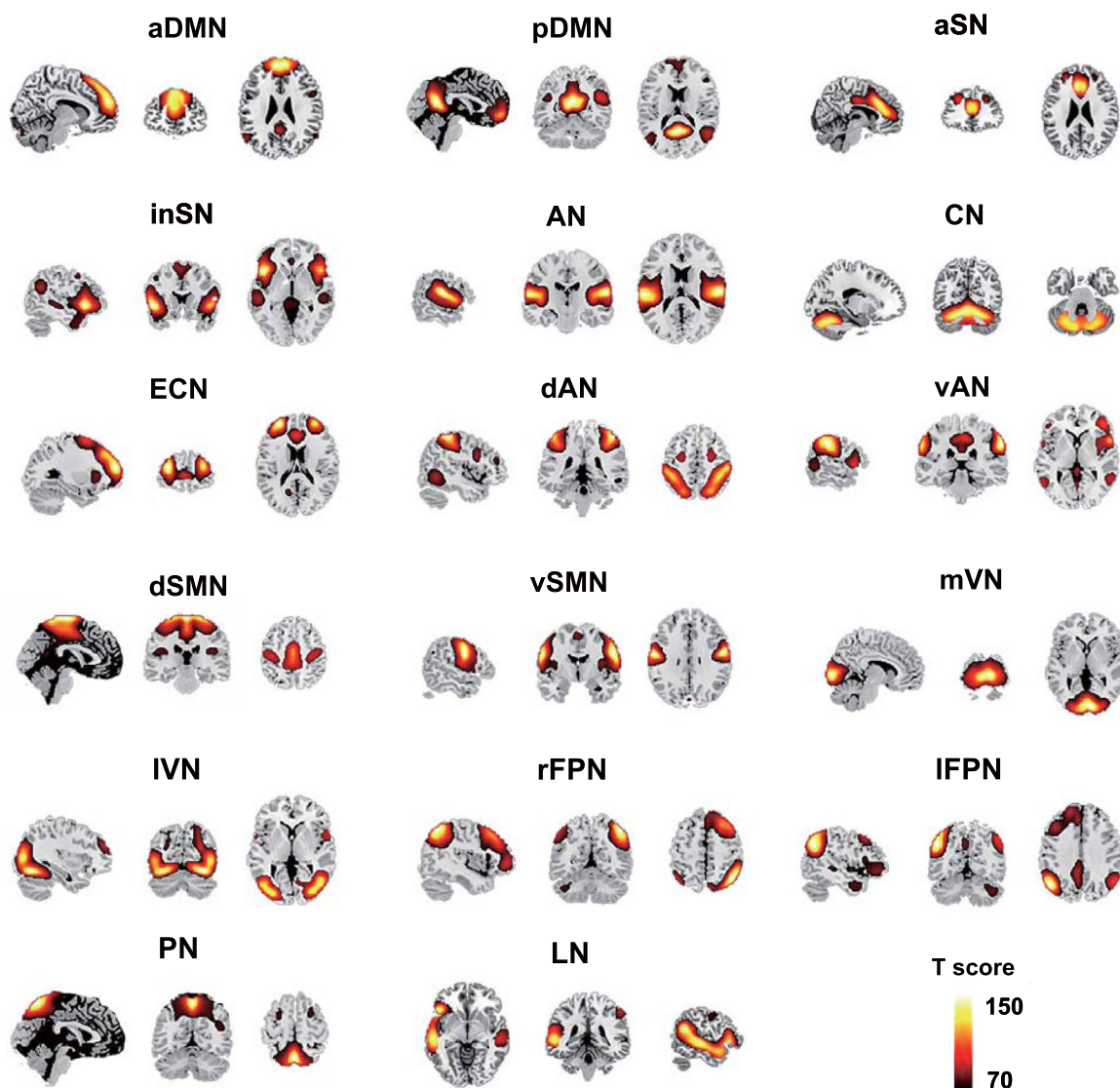
**a.** There are significant associations of lifetime night-time light with the mPFC-ROI GMV (ages of 4–14 years) and SA (5–12 years), WNFC in aDMN (3–11 years) during childhood and adolescence, with cerebellum-ROI GMV (3–7 years), WNFCs in CN (0–6 years), mVN (0–6 years), IVN (3–10 years), BNFCs in aDMN-CN (4–7 years), aDMN-ECN (4–6 years), aDMN-rFPN (4–6 years) and rFPN-IFPN (4–6 years) during childhood in CHIMGEN.

**b.** There are significant associations of lifetime built-up% with the mPFC-ROI GMV (5–16 years) and WNFC in aDMN (4–14 years) during childhood and adolescence, with WNFCs in mVN and IVN (14–20 years) during adolescence, with mPFC-ROI SA (5–7 years), cerebellum-ROI GMV (1–10 years), WNFC in CN (1–10 years), BNFCs in aDMN-CN (4–10 years), aDMN-ECN (5–7 years), aDMN-rFPN (4–10 years) and rFPN-IFPN (4–6 years) during childhood in CHIMGEN.

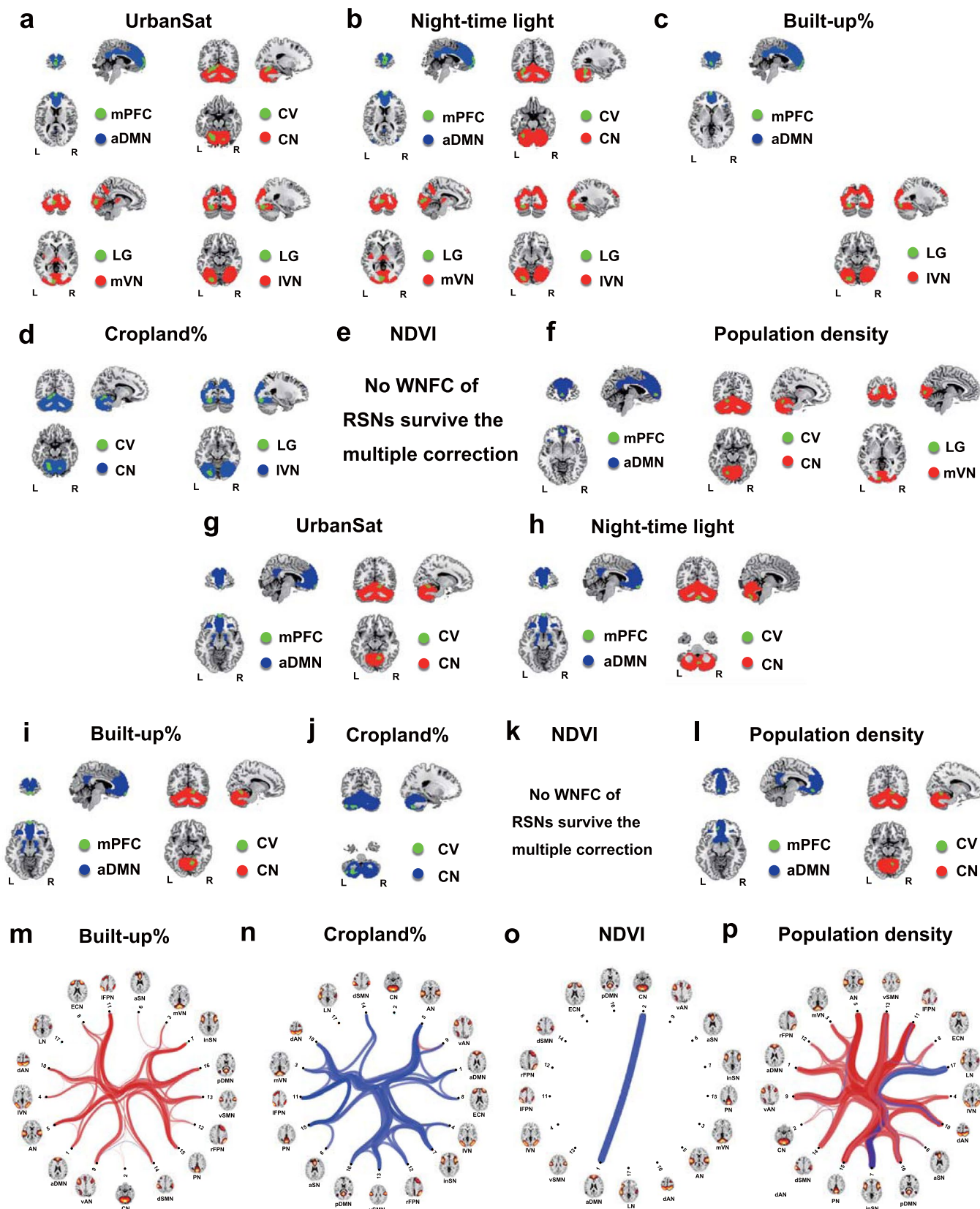
**c.** There are significant associations of lifetime cropland% with the mPFC-ROI GMV (5–15 years) during childhood and adolescence, with mPFC-ROI SA (5–6 years), cerebellum-ROI GMV (4–6 years), WNFCs in aDMN (4–6 years), CN (4–6 years) and IVN (4–10 years), BNFCs in aDMN-CN (0–9 years), aDMN-ECN (2–7 years), aDMN-rFPN (4–10 years) and rFPN-IFPN (4–6 years) during childhood in CHIMGEN.

**d.** We find significant associations of lifetime NDVI with the mPFC-ROI GMV (5–15 years) and BNFC in rFPN-IFPN (6–17 years) during childhood and adolescence, with WNFCs in aDMN (5 years old) and CN (5 years old), BNFCs in aDMN-CN (4–11 years) and aDMN-rFPN (4–10 years) during childhood in CHIMGEN. There are significant correlations of lifetime night-time light (e), built-up% (f), cropland % (g) and NDVI (h) with reaction time for perspective-taking performance during adolescence (ages of 5–16 years for night-time light, 4–17 years for built-up %, 5–19 years for cropland % and 4–17 years for NDVI) in CHIMGEN. Significant correlations of lifetime night-time light (e), built-up % (f), cropland % (g) and NDVI (h) with increasing depression measured by BDI are also observed during childhood in CHIMGEN (0–6 years for night-time light, 2–9 years for built-up %, 0–9 years for cropland % and 3–11 years for NDVI).

The y-axis represents the changes of brain behaviors associated with an increase of interquartile range of individual satellite measures; the x-axis is individual satellite measure lag in ages. Grey areas indicate 95% CIs. A susceptibility window is identified for the ages where the estimated pointwise 95% CI (shaded area) does not include zero. The blue solid lines indicate negative correlations and red ones indicated positive correlations. aDMN, anterior default mode network; BDI, Beck depression index; BNFC, between-network functional connectivity; CN, cerebellar network; CT, cortical thickness; GMV, grey matter volume; IVN, lateral visual network; mPFC, medial prefrontal cortex; mVN, medial visual network; RTpt, reaction time for perspective-taking; SA, surface area; WNFC, within-network functional connectivity.



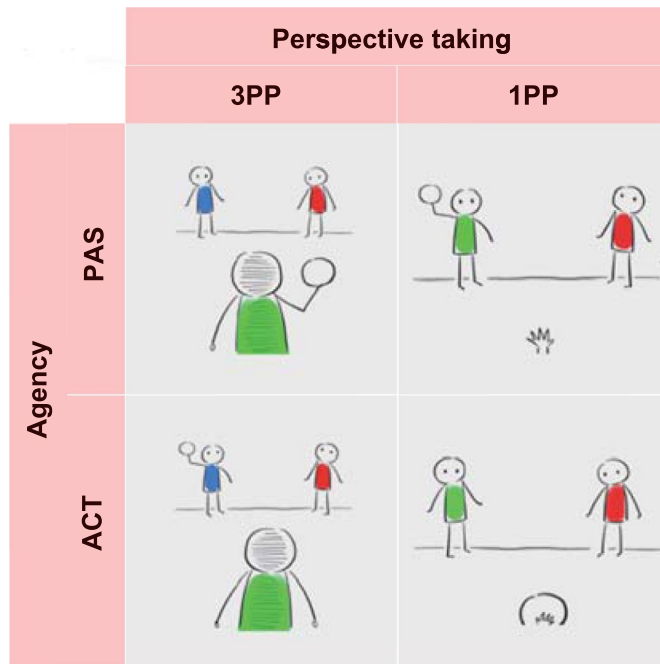
**Extended Data Fig. 8 | Seventeen RSNs identified by independent component analysis in CHIMGEN.** aDMN, anterior default mode network; AN, auditory network; aSN, anterior cingulate cortex part of salience network; CN, cerebellar network; dAN, dorsal attentional network; dSMN, dorsal sensorimotor network; ECN, executive control network; inSN, insular part of salience network; IFPN, left frontal parietal network; LN, language network; IVN, lateral visual network; mVN, medial visual network; pDMN, posterior default mode network; PN, precuneus network; rFPN, right frontal parietal network; RSNs, resting-state networks; vAN, ventral attentional network; vSMN, ventral sensorimotor network.



Extended Data Fig. 9 | See next page for caption.

**Extended Data Fig. 9 | Voxel-wise correlations of individual satellite measures with WNFCs and BNFCs in CHIMGEN (n = 2156) and IMAGEN (n = 315).**

**a-f.** In CHIMGEN, there are negative correlations (blue) of mean UrbanSat (a) and mean night-time light before 18 years (b) with WNFC in the mPFC of the aDMN, positive correlations (red) with WNFCs in the left CV of the CN and left LG of the mVN and IVN (FWE  $P_c < 0.05$ ). **c.** There are negative correlations (blue) of mean built-up% before 18 years with WNFC in the mPFC of the aDMN and positive correlations (red) with WNFC in the left LG of the IVN (FWE  $P_c < 0.05$ ). **d.** There are negative correlations (blue) of mean cropland% before 18 years with WNFCs in the CV of the CN and the left LG of the IVN (FWE  $P_c < 0.05$ ). **e.** There is no correlation of mean NDVI with WNFC of any RSN surviving the multiple correction. **f.** There are negative correlations (blue) of mean population density from GHSL before 18 years with WNFC in the mPFC of the aDMN, positive correlations (red) with WNFCs in the left CV of the CN and the left LG of the mVN (FWE  $P_c < 0.05$ ). **g-l.** In IMAGEN, there are negative correlations (blue) of mean UrbanSat (g), night-time light (h), built-up% (i) before 18 years with WNFC in the mPFC of the aDMN, positive correlations (red) with WNFC in the CV of the CN (FWE  $P_c < 0.05$ ). **j.** There are negative correlations (blue) of mean cropland before 18 years with WNFC in the CV of the CN (FWE  $P_c < 0.05$ ). **k.** There is no correlation of mean NDVI with WNFC of any RSN surviving the multiple correction. **l.** There are negative correlations (blue) of mean population density from GHSL before 18 years with WNFC in the mPFC of the aDMN, and positive correlation (red) with WNFC in the CV of the CN (FWE,  $P_c < 0.05$ ). **m-p.** The mean built-up% (m) ( $N = 32$ ), cropland% (n) ( $N = 41$ ), NDVI (o) ( $N = 1$ ) and population density (p) ( $N = 52$ ) show correlations with BNFCs in CHIMGEN. The red line indicates positive correlations of UrbanSat with BNFCs and blue line indicated negative correlations. N indicates the numbers of significant correlations of BNFCs. aDMN, anterior default mode network; CV, cerebellar vermis; CN, cerebellar network; GHSL, global human settlement layers; LG, lingual gyrus; IVN, lateral visual network; mPFC, medial prefrontal cortex; mVN, medial visual network; NDVI, normalized difference vegetation index; WNFC, within-network functional connectivity.



**Extended Data Fig. 10 | The schematic summary of ball tossing game task design, which measures perspective taking and agency performance.** ACT, active agency; 1PP, first-person perspective; 3PP, third-person perspective; PAS, passive agency.

## Reporting Summary

Nature Research wishes to improve the reproducibility of the work that we publish. This form provides structure for consistency and transparency in reporting. For further information on Nature Research policies, see our [Editorial Policies](#) and the [Editorial Policy Checklist](#).

### Statistics

For all statistical analyses, confirm that the following items are present in the figure legend, table legend, main text, or Methods section.

n/a Confirmed

- The exact sample size ( $n$ ) for each experimental group/condition, given as a discrete number and unit of measurement
- A statement on whether measurements were taken from distinct samples or whether the same sample was measured repeatedly
- The statistical test(s) used AND whether they are one- or two-sided  
*Only common tests should be described solely by name; describe more complex techniques in the Methods section.*
- A description of all covariates tested
- A description of any assumptions or corrections, such as tests of normality and adjustment for multiple comparisons
- A full description of the statistical parameters including central tendency (e.g. means) or other basic estimates (e.g. regression coefficient) AND variation (e.g. standard deviation) or associated estimates of uncertainty (e.g. confidence intervals)
- For null hypothesis testing, the test statistic (e.g.  $F$ ,  $t$ ,  $r$ ) with confidence intervals, effect sizes, degrees of freedom and  $P$  value noted  
*Give  $P$  values as exact values whenever suitable.*
- For Bayesian analysis, information on the choice of priors and Markov chain Monte Carlo settings
- For hierarchical and complex designs, identification of the appropriate level for tests and full reporting of outcomes
- Estimates of effect sizes (e.g. Cohen's  $d$ , Pearson's  $r$ ), indicating how they were calculated

*Our web collection on [statistics for biologists](#) contains articles on many of the points above.*

### Software and code

Policy information about [availability of computer code](#)

Data collection

In CHIMGEN and IMAGEN datasets, Google earth engine was applied to collect the physical environment data (nightlight, NDVI, NDBI, NDWI, global land cover mapping) based on the subjects' geolocation. T1-weighted imaging, diffusion tensor imaging and resting-state functional imaging were acquired using 3.0 Tesla MRI scanners at each center. And paper-based questionnaire and E-Prime 2.0 software was used to collect some of behavioral data.

Data analysis

R package lavaan, R package mice, R package meto, MATLAB and SPSS was used to analysis remote sensing data for physical environment and behavioral data. And Statistical Parametric Mapping software package (SPM12), FMRIB's Software Library (FSL v6.0.1) toolbox, Freesurfer, Data Processing Assistant for Resting-State fMRI (DPARSFA) and Group ICA Of fMRI Toolbox (GIFT) were used to analysis neuroimaging data.

For manuscripts utilizing custom algorithms or software that are central to the research but not yet described in published literature, software must be made available to editors and reviewers. We strongly encourage code deposition in a community repository (e.g. GitHub). See the Nature Research [guidelines for submitting code & software](#) for further information.

### Data

Policy information about [availability of data](#)

All manuscripts must include a [data availability statement](#). This statement should provide the following information, where applicable:

- Accession codes, unique identifiers, or web links for publicly available datasets
- A list of figures that have associated raw data
- A description of any restrictions on data availability

The raw remote sensing data are free access from Google earth engine. The raw neuroimaging data and behavioral data that support the findings of this study are available from the corresponding author upon reasonable request. These data were used to generate images in Table 1 ,Figs. 1-5, all supplementary Tables and Figs.

# Field-specific reporting

Please select the one below that is the best fit for your research. If you are not sure, read the appropriate sections before making your selection.

Life sciences       Behavioural & social sciences       Ecological, evolutionary & environmental sciences

For a reference copy of the document with all sections, see [nature.com/documents/nr-reporting-summary-flat.pdf](http://nature.com/documents/nr-reporting-summary-flat.pdf)

## Life sciences study design

All studies must disclose on these points even when the disclosure is negative.

### Sample size

1. UrbanSat  
CHIMGEN: n=3306;  
IMAGEN:n=561;
2. Participants with remote sensing data and neuroimage data:  
CHIMGEN:  
GMV (n=2176); CT and SA (n=2164);TBSS (n=2158);WNFC and BNFC (n=2156)  
IMAGEN:  
GMV(FU2,n=415; BL-FU2=340); CT and SA (FU2,n=420;BL-FU2, n=325); TBSS (FU2, n=436;BL-FU2, n=321); WNFC and BNFC (FU2, n=351;BL-FU2,n= 83);
3. Participants with remote sensing data and behavioral data  
CHIMGEN:  
CVLT-II (n=2173); N-back(n=2063);SDMT(n=2139); PT(n=2148); Go/no-go(n=2024); Depression(n=2170); Anxiety(n= 2170)  
IMAGEN:  
PT(n=342); Depression(n=346); Anxiety(n=447; n=391)

### Data exclusions

- CHIMGEN:
- (1) Excluding participants without lifetime residential information  
Among the 5425 participants, 3336 participants had provided lifetime residential geographies. The remaining 2089 participants were excluded because they only provided their residential addresses at the time point of recruitment but they refused to provide their residential addresses at any other time points since birth. From the 3336 participants, we successfully extracted satellite-based measures of urbanicity of 3306 participants. The other 30 participants were excluded because extracting satellite measures failed in more than three years during their lifetime.
  - (2) Excluding participants without confounding covariates  
Potentially confounding covariates including age, gender, education, site, body mass index (BMI), genetic population stratification, socioeconomic status (SES), total intracranial volume (TIV), mean cortical thickness (MCT) and total surface area (TSA) were corrected in the correlation analyses of satellite based-measure of urbanicity with brain and behavior. Complete information of confounders was available in 2176 participants, with 1130 participants being excluded from the 3306 participants with lifetime geopositioned data.
  - (3) Excluding participants without qualified neuroimaging data  
For each neuroimaging measure, we had to exclude participants with unqualified raw imaging data and participants failed to pass the quality control (QC) during imaging data preprocessing. In the 2176 participants, 2176 participants were included in the voxel-based morphometry (VBM) analysis of gray matter volume (GMV) and 2164 participants in the surface-based morphometry (SBM) analysis of cortical thickness (CT) and surface area (SA) based on T1-weighted neuroimaging data ; 2158 participants in the Tract-based Spatial Statistics (TBSS) analysis of fractional anisotropy (FA) based on diffusion tensor imaging (DTI) data; and 2156 participants in the within-network (WNFC) and between-network (BNFC) functional connectivity analyses based on resting-state functional MRI (rsfMRI) data.
  - (4) Excluding participants without qualified behavioral assessments  
For each behavioral measure analysis, we had to exclude participants without qualified behavioral assessment. In the 2176 participants with at least one type of the qualified MRI data, 2173 participants were finally included in the analysis of verbal learning memory, 2063 in working memory, 2139 in information processing speed, 2148 in social cognition, 2024 in cognitive control, and 2170 in mental health.
- IMAGEN:
- (1) Excluding participants without lifetime residential information  
Among the 1411 participants of IMAGEN-FU2, 561 participants provided lifetime residential geographies. All participants's satellite-based measures of urbanicity at each year have been extracted successfully.
  - (2) Excluding participants without confounding assessments  
From these 561 participants, we excluded 79 participants without the confounding assessments (SES, parental history of mental illness and genetic population stratification) and the remaining 482 participants were included in the further analysis.
  - (3) Excluding participants without qualified neuroimaging data  
Among the remaining 482 participants (FU2), 415 participants were included in VBM analysis after passing QC; 420 participants in SBM analysis; 436 participants in TBSS analysis; and 351 participants in WNFC and BNFC analyses. Participants with both BL (age 14) and FU2 (age 19) imaging data after QC were used in brain development analyses, including 340 participants in VBM analysis, 325 participants in SBM analysis, 396 participants in TBSS analysis, and 83 participants in WNFC and BNFC analyses. It is notable that during IMAGEN baseline assessment in the year of 2009, resting state MRI was only carried out in 156 participants.
  - (4) Excluding participants without qualified behavioral assessments  
Among the 482 participants (FU2), complete data of perspective taking was available in 342 participants, Ruminating Scale Questionnaire (RSQ) in 346 participants, Generalized Anxiety Scale from The Development and Well-Being Assessment Interview (DAWBA-GA) in 447 participants and Anxiety Screening for Composite International Diagnostic Interview (CIDI-DIA) in 391 participants.

### Replication

- The results from CHIMGEN could be replicated in IMAGEN datasets

Randomization	Our study aims to test the effect of global urbanicity on brain development and behaviors. We don't have group allocation
Blinding	Our study aims to test the effect of global urbanicity on brain development and behaviors. We don't have group allocation

## Reporting for specific materials, systems and methods

We require information from authors about some types of materials, experimental systems and methods used in many studies. Here, indicate whether each material, system or method listed is relevant to your study. If you are not sure if a list item applies to your research, read the appropriate section before selecting a response.

### Materials & experimental systems

- |                                     |                               |
|-------------------------------------|-------------------------------|
| n/a                                 | Involved in the study         |
| <input checked="" type="checkbox"/> | Antibodies                    |
| <input checked="" type="checkbox"/> | Eukaryotic cell lines         |
| <input checked="" type="checkbox"/> | Palaeontology and archaeology |
| <input checked="" type="checkbox"/> | Animals and other organisms   |
| <input type="checkbox"/>            | Human research participants   |
| <input checked="" type="checkbox"/> | Clinical data                 |
| <input checked="" type="checkbox"/> | Dual use research of concern  |

### Methods

- |                                     |                        |
|-------------------------------------|------------------------|
| n/a                                 | Involved in the study  |
| <input checked="" type="checkbox"/> | ChIP-seq               |
| <input checked="" type="checkbox"/> | Flow cytometry         |
| <input type="checkbox"/>            | MRI-based neuroimaging |

## Human research participants

### Policy information about [studies involving human research participants](#)

#### Population characteristics

CHIMGEN:  
n=3306;  
age(mean/SD)=24.00/3.00  
Male/Femal=1213/2093  
IMAGEN:  
n= 561  
age(mean/SD)=18.74/0.97  
Male/Female=254/307

#### Recruitment

CHIMGEN project has 31 centers, IMAGEN project has 8 centers. The written informed consent is obtained from each participant of two datasets.

#### Ethics oversight

The CHIMGEN and IMAGEN project were approved by the ethic committee of each sub-center.

Note that full information on the approval of the study protocol must also be provided in the manuscript.

## Magnetic resonance imaging

### Experimental design

#### Design type

In CHIMGEN and IMAGEN datasets, T1-weighted imaging, diffusion tensor imaging and resting-state functional imaging were acquired using 3.0 Tesla MRI scanners.

#### Design specifications

Please see the below sequence & imaging parameters

#### Behavioral performance measures

1. Verbal learning memory (California verbal learning test)
  2. Working memory (N-back test)
  3. Information processing speed (Symbols Digit Modality Test )
  4. Social cognition
- CHIMGEN: In Ball tossing game, we record the accuracy and reaction time in perspective taking session and agency session, respectively;
- IMAGEN: perspective taking, fantasy, empathic concern and personal distress score from Interpersonal Reactivity Index (IRI) questionnaire was recorded;
5. Executive control (Go-No go test)
  6. Mental health
- CHIMGEN: Beck Depressive Inventory and State-Trait Anxiety Inventory
- IMAGEN: Ruminating Scale, International Diagnostic Interview and The Development and Well-Being Assessment Interview

## Acquisition

Imaging type(s)	structural, diffusional and functional
Field strength	3.0 Tesla
Sequence & imaging parameters	<p>CHIMGEN:</p> <p>1. T1 weighted images acquisition. For the Discovery™ MR750 scanner, sagittal high-resolution three-dimensional T1-weighted imaging were acquired by Brain Volume imaging (3D-BRAVO) series with the following parameters: repetition time (TR)/echo time (TE) = 8.14/3.17 ms; inversion time (TI) = 450 ms; field of view (FOV) = 256mm × 256 mm; matrix = 256 × 256; flip angle (FA) = 12°; slice thickness (ST) = 1 mm; no gap; 188 sagittal slices. For the TrioTim Verio Skyra scanner, sagittal high-resolution three-dimensional T1-weighted imaging data were acquired by magnetization prepared gradient-echo (MP-RAGE) series with the following parameters: TR/TE = 2000/3.44 ms; TI = 900 ms; FOV = 256mm × 256 mm; matrix = 256 × 256; FA = 9°; ST = 1 mm; no gap; 192 sagittal slices;</p> <p>2. Diffusion tensor images (DTI) acquisition</p> <p>For the Discovery™ MR750 scanner, diffusion tensor images were acquired using spin-echo single-shot diffusion tensor echo planar imaging (SE-SS-DT-EPI) sequence with the following parameters: TR/TE = 6000/61 ms; FOV = 256mm × 256 mm; matrix = 128 × 128; FA = 90°, ST = 3 mm; no gap; 50 axial slices; 64 diffusion gradient directions with b-value 1000 s/mm<sup>2</sup>; 5 non-diffusion-weighted images (b=0s/mm<sup>2</sup>); For the TrioTim Verio Skyra scanner diffusion tensor images were also acquired using the SE-SS-DT-EPI with the following parameters: TR/TE = 6500/89 ms; FOV = 256mm × 256 mm; matrix = 128 × 128; FA = 90°, ST = 3 mm; no gap; 50 axial slices; 64 diffusion gradient directions with b-value 1000 s/mm<sup>2</sup>; 1 non-diffusion-weighted images (b=0s/mm<sup>2</sup>).</p> <p>3. Resting-state fMRI acquisition</p> <p>For the Discovery™ MR750 scanner, resting-state functional MRI data were collected using gradient-echo single-shot echo-planar imaging (GRE-SS-EPI) with the following parameters: TR/TE = 2000/30 ms; FOV = 220mm × 220 mm; matrix = 64 × 64; FA = 90°; ST = 3 mm; gap=1mm; 40 interleaved transverse slices; 180 volumes. For the TrioTim Verio Skyra scanner, resting-state functional MRI data were also collected using GRE-SS-EPI with the following parameters: TR/TE = 2000/30 ms; FOV = 220mm × 220 mm; matrix = 64 × 64; FA = 90°; ST = 3 mm; gap=0.99 mm; 36 interleaved transverse slices; 180 volumes.</p> <p>IMAGEN:</p> <p>1. T1 weighted images acquisition</p> <p>High resolution sagittal three-dimensional T1 weighted MP-RAGE images were acquired according to the ADNI protocol (<a href="http://adni.loni.usc.edu/methods/mri-analysis/mri-acquisition/">http://adni.loni.usc.edu/methods/mri-analysis/mri-acquisition/</a>) with the following standardized parameters across sites: TR/TE = 2300/2.8 ms; FA = 8°; matrix = 256×256; 160 volumes.</p> <p>2. DTI acquisition</p> <p>DTI were acquired using spin-echo single-shot diffusion tensor echo planar imaging (SE-SS-DT-EPI) series with the following parameters: TR/TE = 6000/104 ms; FOV = 256mm × 256 mm; matrix = 128 × 128; FA = 90°, ST = 3 mm; no gap; 60 axial slices; 32 diffusion gradient directions with b-value 1300 s/mm<sup>2</sup>.</p> <p>3. Resting-state fMRI acquisition</p> <p>Resting state fMRI scanning of the IMAGEN subjects were carried out at multiple sites with the following parameters: TR/TE = 2220/30ms; FOV = 218mm × 218mm; matrix = 64× 64; FA = 75°; ST = 2.4 mm; gap=3.4 mm; 164 volumes.</p>
Area of acquisition	A whole brain scan
Diffusion MRI	<input checked="" type="checkbox"/> Used <input type="checkbox"/> Not used
Parameters	<p>CHIMGEN:</p> <p>For the Discovery™ MR750 scanner, diffusion tensor images were acquired using spin-echo single-shot diffusion tensor echo planar imaging (SE-SS-DT-EPI) sequence with the following parameters: TR/TE = 6000/61 ms; FOV = 256mm × 256 mm; matrix = 128 × 128; FA = 90°, ST = 3 mm; no gap; 50 axial slices; 64 diffusion gradient directions with b-value 1000 s/mm<sup>2</sup>; 5 non-diffusion-weighted images (b=0s/mm<sup>2</sup>); For the TrioTim Verio Skyra scanner diffusion tensor images were also acquired using the SE-SS-DT-EPI with the following parameters: TR/TE = 6500/89 ms; FOV = 256mm × 256 mm; matrix = 128 × 128; FA = 90°, ST = 3 mm; no gap; 50 axial slices; 64 diffusion gradient directions with b-value 1000 s/mm<sup>2</sup>; 1 non-diffusion-weighted images (b=0s/mm<sup>2</sup>).</p> <p>IMAGEN:</p> <p>DTI were acquired using spin-echo single-shot diffusion tensor echo planar imaging (SE-SS-DT-EPI) series with the following parameters: TR/TE = 6000/104 ms; FOV = 256mm × 256 mm; matrix = 128 × 128; FA = 90°, ST = 3 mm; no gap; 60 axial slices; 32 diffusion gradient directions with b-value 1300 s/mm<sup>2</sup>.</p>

## Preprocessing

Preprocessing software	<ol style="list-style-type: none"> <li>Gray matter volume (GMV) calculation based on T1 weighted image: Computational Anatomy Toolbox (CAT12 v1364) (<a href="http://dbm.neuro.uni-jena.de/cat">http://dbm.neuro.uni-jena.de/cat</a>) implemented in Statistical Parametric Mapping (SPM12) software package (<a href="http://www.fil.ion.ucl.ac.uk/spm">http://www.fil.ion.ucl.ac.uk/spm</a>)</li> <li>Cortical thickness and surface area based on T1 weighted image: Freesurfer v6.0.0 (<a href="http://surfer.nmr.mgh.harvard">http://surfer.nmr.mgh.harvard</a>)</li> <li>Tract based spatial statistics (TBSS) calculation based on DTI data: FSL v6.0.1 toolbox was used both in CHIMGEN and IMAGEN.</li> <li>Within- and between functional network connectivity (WFNC and BNFC) calculation based on resting-state functional imaging data:</li> </ol> <p>CHIMGEN:</p> <p>Data Processing Assistant for Resting-State fMRI (DPARSFA) v4.4</p> <p>IMAGEN:</p>
------------------------	---

FSL v5.0.9 and Advanced Normalization Tools (ANTS v1.9.2)  
 Group ICA Of fMRI Toolbox (GIFT) software v4.0 was used to construct brain functional network in both datasets.

#### Normalization

Non-linear

#### Normalization template

1. Gray matter volume (GMV) calculation based on T1 weighted image: Montreal Neurological Institute (MNI) space;
2. Tract based spatial statistics (TBSS) calculation based on DTI data: MNI space
3. Resting-state functional MRI data: standard echo planar image (EPI) template

#### Noise and artifact removal

1. Gray matter volume (GMV) calculation based on T1 weighted image: correct for variance in individual brain sizes;
2. Tract based spatial statistics (TBSS) calculation based on DTI data: correct for eddy currents and subject movement
3. Resting-state functional MRI data: correct for six rigid-body realignment parameters and average BOLD signals of the whole brain and ventricular and white matter regions

#### Volume censoring

Rigid realignment was performed to estimate and correct the motion displacement. Subjects had a maximum displacement in one or more of the orthogonal directions (x, y, z) of > 2 mm or a maximum rotation (x, y, z) > 2.0° were excluded.

### Statistical modeling & inference

#### Model type and settings

For the remote sensing data, confirmatory factor model was applied to construct UrbanSat, a index for urbanicity. For the relation between UrbanSat and neuroimaging, multiple regression model was applied. For the relation between UrbanSat and behaviours, spearman correlation was applied. For the relation between UrbanSat, brain and behaviour, multiple mediation analysis was applied.

#### Effect(s) tested

Comparative Fit Index (CFI), Akaike(AIC), sample-size adjusted Bayesian(BIC), root mean square error of approximation (RMSEA), standard root mean square residual (SRMR), Tucker-Lewis index (TLI), T value , effect size Phi value, effect size r coefficient, r value, SE, 95% CI, z value and I2 statistics in meta analysis, Spearman rho value

Specify type of analysis:  Whole brain  ROI-based  Both

Statistic type for inference  
 (See [Eklund et al. 2016](#))

voxel-wise

#### Correction

FWE correction, TFCE non-parameter correction and permutation test

### Models & analysis

n/a Involved in the study

- |                                     |  |
|-------------------------------------|--|
| <input type="checkbox"/>            | <input checked="" type="checkbox"/> Functional and/or effective connectivity |
| <input checked="" type="checkbox"/> | <input type="checkbox"/> Graph analysis                                      |
| <input checked="" type="checkbox"/> | <input type="checkbox"/> Multivariate modeling or predictive analysis        |

Functional and/or effective connectivity

partial correlation